People's Democratic Republic of Algeria
Ministry of Higher Education and Scientific Research
TissemsiltUniversity

Faculty of Sciences and Technology
Department of Sciences and Technology

Dissertation submitted in fulfillment of the requirements for the degree of academic Master in

Stream: **Mechanical Engineering**

Specialty: **Energy Installations and Turbomachines**

Realized by: **MELAAB Ahmed**

Theme

Numerical study of the flow behavior over cylinders with geometrical shape modification

---

September 2021

Board of Examiners:

Dr. KAHIL Y.	Supervisor	Tissemsilt University
Dr. BENLEKKAM M.	Examiner	Tissemsilt University
Dr. BENLEFKI A.	Examiner	TissemsiltUniversity

2020-2021

République Algérienne Démocratique et Populaire
Ministère de l'Enseignement Supérieur
et de la Recherche Scientifique
Université de Tissemsilt
Faculté des Sciences et de la Technologie
Département des Sciences et de la Technologie

Mémoire de fin d'études pour l'obtention du diplôme de Master académique en

Filière:**Génie Méchanique**

Spécialté: **Installations Energétique et Turbomachines**

Réalizé par: **MELAAB Ahmed**

Thème

Etude Numérique du comportement d'écoulement autour des cylindres avec la modification des formes géométriques

---

Septembre 2021

Devant le Jury:

Dr. KAHIL Y.	Encadrant	Université de Tissemsilt
Dr. BENLEKKAM M.	Examinateur	Université de Tissemsilt
Dr. BENLEFKI A.	Examinateur	Université de Tissemsilt

Année universitaire : 2020-2021

Dedication

“Everything I am or ever will be, I owe it to my mother

My success is because of her prayer for me

To you mother.

“To my biggest supporter

To you father “

To all my family

Acknowledgments

All the gratitude and thanks to Allah our creator who has given us the strength to carry out and complete this work.

First of all, I would like to thank the members of the jury, the president ***Dr. BENLEKKAM M****. and* ***Dr. BENLEFKI A****.to agree to examine this modest memory.*

I would like to thank my promoter very warmly ***Dr. KAHIL Y.*** *for having proposed this subject to me, for its precious advice for his open-mindedness and availability.*

Many thanks to all the professors of the department of Sciences and Technology for their contributions to my education and training, and my knowledge.

TABLE OF CONTENTS

List of figures

List of tables

Nomenclature

D	Diameter
L	Length
λ/Dm	Wavelength ratio
a/Dm	Amplitude ratio
T/D	Pitch diameter ratio
M	Mass
ρ	fluid density[kg/m^3]
U	mean fluid velocity[$m.s^{-1}$]
P	Pressure
$\vec{A}$	surface area vector
C_{μ}	constants of the K-ε model
μ	dynamic viscosity of the fluid [$P_a s^{-1}$]
u′	fluctuating component
N	grid number
Re	Reynolds number
$\overline{u}$	time-averaged velocity
s_{ij}	train-rate tensor
v_T	turbulent eddy viscosity
k	turbulence kinetic energy
v	molecular viscosity
$\overline{v}$	transport equations
C_{w1}	ω production
Ω_{ij}	rotation tensor
$C_{\varepsilon 1}, C_{\varepsilon 2}, \delta_k, \delta_\varepsilon$	coefficients of k-ε modeling
$\overline{u_i' u_j'}$	components of Reynolds tensor.
$\alpha, \beta_0^*, \sigma, \sigma^* \beta_0, \sigma_{do}$	coefficients of k-ω modeling
P_k	production limiter
F_1	blending function
F_2	second blending function
$\beta^*, \alpha_1, \beta_1, \sigma_{k1}, \sigma_{\omega 1}, \alpha_2, \sigma_{k2}, \sigma_{\omega 2}$	coefficients of k-ω-SST model
$\vec{v}$	velocity vector $\left(\vec{v} = v_x \vec{\imath} + v_y \vec{\jmath}\right)$
G	Gap distance
H	

S	Thickness
h	Groove width
$U/U0$	Groove depth
$V/U0$	Mean streamwise velocity
$\overline{C_P}$	Mean cross-stream velocity
$\bar{P}$	Mean pressure coefficient
P_∞	Mean pressure
u_∞	Initial pressure
	Initial velocity

GENERAL INTRODUCTION

General introduction:

Turbulence, a scientific term, is used to describe some complex and unpredictable movement of fluids. It has been part of our daily experience for a long time. You don't need any telescope or microscope to contemplate the volutes of cigarette smoke, elegant arabesques of cream poured over the coffee, and the vigorous swirls of a mountain stream. We sometimes experience outbursts of "clear air turbulence" in an airplane. Ultrasound can reveal turbulent blood flow in our arteries.

With the development of modern computers, numerical methods have been developed and are now used to solve complex fluid dynamics problems (turbulence) in a short period of time. These computers can be used to execute CFD codes that can easily handle complex flow projects. This allows us to get results faster. Computational fluid dynamics (CFD) is one of the most emerging fields in applied science. And has become the tool of choice for solving problems involving one or more of the following phenomena: fluid flow, heat transfer, mass transfer, and chemical reactions.

As known that the fundamental and one of the most studied problems in computational fluid mechanics is flow around a circular cylinder. Therefore we will Study flow over a single cylinder, with three shape different (smooth, grooved and with plat). We will mention the effect of grooves and splitter plate. And we will compare the results with experimental results.

The manuscript is divided into five chapters. We start with bibliographic analysis; Chapter 2 deals with turbulence modeling. In Chapter 3, concerns the numerical resolution of all free software used for this work. Chapter 4 presents the case study, followed by the results and discussion. Finally, we conclude with a general conclusion that brings together the main points of our research.

CHAPTER 1: BIBLIOGRAPHIC ANALYSIS

Introduction

Studying the flow around a circular cylinder is fundamental and one of the most studied problems in fluid mechanics and aerodynamics. In this chapter, we present a bibliographic synthesis covering several works done in this field.

H. L. Zhang et al (1996) [1] investigated unstable and incompressible flow fields around smooth and grooved cylinders. A new boundary condition has been proposed on the surface of a grooved roll so that the Navier-Stokes solver code originally developed for smooth cylindrical flow could be slightly modified to simulate the flow field around a grooved roll. A detailed comparison of the smooth and grooved cylindrical flow shows that the grooves affect the flow characteristics of the cylindrical surface and the flow structure in space.

J.Kim and H.Choi (2002) [2] performed a three-dimensional numerical simulation to control the flow around a cylinder with a Reynolds number of 40to 3900. A distributed force is applied on the surface of the cylinder, and the profile from the stagnation point $\pm 90°$ (blow/suction) changes sinusoidally in the span direction and is fixed in time. The phase difference between the forced velocities from the upper and lower surfaces of the cylinder is set to zero (in phase) or π (out of phase). The results show that the in-phase distribution force significantly weakens the vortex shedding and reduces the resistance under laminar and turbulent flow conditions. We also found that in order to minimize drag, there is an optimal spanwise wavelength, which depends on the Reynolds number.

M.Rahmanet al. (2007) [3] numerically studied and physically analyzed the dynamic characteristics of the pressure and velocity fields of unstable incompressible laminar flow and turbulent wakes behind a cylinder. The governing equations written in the velocity pressure formula are solved using the two-dimensional finite volume method. The initial mechanism of vortex shedding was demonstrated, and unstable physical strength was evaluated. The turbulence of $Re = 1000 \,\&\, 3000$ is simulated using $k - \varepsilon$ standard, $k - \varepsilon$ Realizable and $k - \omega$ SST turbulence models. The ability of these turbulence models to calculate lift and drag coefficients is also verified. The theoretically obtained drag and lift oscillation frequencies are in good agreement with the experimental results.

S.E. Ravazi et al(2008)[4] Conducted a study of the effect of the distributor plate length on the flow forces and heat transfer behavior of a round cylinder at low Reynolds numbers ($20 \leq Re \leq 1000$) using the finite volume methodology on a triangular unstructured mesh. A significant reduction in the drag coefficient as well as the mean Nusselt number was observed in the presence of a divider plate, stabilizing the wake area and thus reducing vortex rejection. However, the

conductive heat transfer was increased due to the additional heat transfer area generated by the separation plate on which the overall heat transfer in the system was improved.

K.Lam and Y.F.Lin(2008) [5] used the large eddy simulation (LES) to study the cross flow around wavy cylinders with wavelength ratio $\lambda/D_m = 1.036\ to\ 3.33$at $Re = 3000$. The average flow field and near-wake structure are given, and compared with the cylinder under the same Reynolds number. The results showed that the mean drag coefficients of the wavy cylinders are less than those of a corresponding circular cylinder due to a longer wake vortex formation length generated by the wavy cylinders. For a subcritical Reynolds number of 3000, a maximum drag coefficient reduction of up to 18% compared with a circular cylinder is obtained corresponding to an optimal wavelength ratio of λ/D_m around 1.9 and an amplitude ratio $a/Dm$of 0.152. The fluctuating lift coefficients of the wavy cylinders are also greatly reduced or even suppressed.

I. Afganet al. (2011) [6] studied the numerical modeling of flow around a single and two side-by-side infinite cylinders. For a single cylinder, the Reynolds number based on diameter and free flow velocity is 3900. Extrusion length, wall mesh refinement, convection scheme and sub-grid scale (SGS) model based on the span direction. It is found that the average solution is not affected by the extrusion length of more than 4 diameters or the upward winding of 1%. However, coarsening the grid in the wall normal direction or turning off the sub-grid scale model will have a huge impact on the recirculation length and basic velocity field. In the case of a Reynolds number of 3000, a series of pitch diameter ratio tests ($T/D = 1.0, 1.25 \leq T/D \leq 5.0$) were performed on two side-by-side cylinders.For the intermediate pitch to diameter ratios ($1{:}25 \leq T/D \leq 1{:}75$),multiple shedding frequencies were detected with a biased wake flow deflection. Furthermore, this biased flow deflection was found to be bistable, i.e., it changes the direction (flipping over)intermittently from one side to the other.

O. Ladjedel et al (2011) [7] conducted experimental and numerical studies on the reduction of the Drag of grooved cylinders. The experiment was conducted in a closed-loop subsonic wind tunnel (TE44); in the numerical study, the ANSYS FLUENT code was used to solve the Reynolds Navier-Stokes equation (RANS). $The\ k-\varepsilon$ and $k-\omega\ SST$ models were tested. The obtained results show:

The reduction in pressure drag is due to the decreasing pressure on the front surface of the cylinder and the backward movement of the cylinder separation point.The form of drag is reduced due to the use of grooves.

P.Badami et al(2012) [8]studied flow around circular cylinder and cylinder with rectangular and triangular wake splitter. The flow around the cylinders is performed at Reynolds number$R_e = 5, 20, 40, 50, 80\ and\ 100$, and length of wake splitter in both configurations is taken to be equal to diameter of cylinder. Wake length is found to be less with rectangular wake splitter when compared to bare cylinder and cylinder with triangular wake splitter. Coefficient of drag is found to be less for triangular wake splitter when compared to bare cylinder & cylinder with rectangular wake splitter.

T. Yahiaoui et al(2013) [9]the drag reduction experiment was carried out on the in-line tube bundle with a$7 * 7$ structure and a pitch ratio of 1.44. Two longitudinal grooves are placed on the outer surface of the cylinder as passive control. The experiment was conducted using a subsonic wind tunnel. Use multi-channel differential pressure to measure pressure distribution along various azimuth angles of the tube. Resistance can also be determined using a combined linear strain gauge balance. The pressure drop is derived from the resulting resistance. The results obtained showed that the pressure drop of the tube bundle was unexpectedly reduced. Compared with the configuration without grooves, the pressure drop with a Reynolds number of $1.33 * 10^4$ is reduced by 36.5%. Some correlations of pressure drop are proposed.

L. Zou et al (2013) [10] Conducted extensive numerical studies on the $3 - D$ laminar flow around two wavy cylinders arranged in series. The spacing ratio ($^L/_{Dm}$) ranges from 1.5 to 5.5, and the Reynolds number is 100. The focus of the investigation is the spacing ratio ($^L/_{Dm}$) and the wave surface, force and pressure coefficients on the $3 - D$ near wake mode, and the vortex shedding frequency of two series wave cylinders. The flow around two cylinders in series was also obtained for comparison. The spacing ratio is in the range of $^L/_D = 1.5, 5.5\ m$. Unlike two series cylinders, the wave cylinders arranged in series do not have three basic types of wake interference behavior. Compared with the upstream cylinder, the vortex shedding behind the upstream wave cylinder occurs more downstream. This leads to a reduction in the effect of cylinder vibration and a significant reduction in drag. When $^L/_{Dm} = 4.0$, the drag reduction and vibration control effects of the two series wave cylinders become more and more obvious, and the two series cylinders appear obvious vortex shedding in the upstream cylinder state.

O. Ladjedel et al (2014) [11] studied the influence of longitudinal grooves on pipes with three Reynolds numbers in series. The outer surface of each cylinder has two grooves at 90° and 270° angles. The experiment was conducted using a subsonic wind tunnel. The pressure distribution along the pipeline is determined for changes in azimuth from 0 degrees to 360 degrees. Drag and lift are measured with TE 44 balance. The results show that:

- ❖ The absolute value of the pressure coefficient increases as the Reynolds number increases.
- ❖ Compared with the downstream cylinder, the upstream cylinder has a greater resistance pressure.
- ❖ The pressure distribution trend of the two cylinders seems to be the same as that of the isolated cylinder.
- ❖ When a grooved cylinder is used, the resistance pressure of high Reynolds number will be reduced.

A.Inamdar and R.Kumar (2015) [12] performed a numerical study of flow structure around a cylinder with V-shaped grooves. In the range of $ReD = 2 * 10^4$, based on the cylinder diameter ($D = 40mm$), the drag coefficient and turbulence statistics data of the wake behind each cylinder are analyzed. The V-shaped groove reduces the drag coefficient acting on the cylinder by 28.47%. When $ReD = 2 * 10^4$, compared with a smooth cylinder under the same Reynolds number.

L. Kai et al (2016) [13] conducted an experimental study to investigate the effect of the splitter plate on the downstream wake of a cylinder symmetrically placed in a restricted channel. Use particle image velocimetry (PIV) measurements to visualize the flow structure and analyze changes in the vortex shedding process. The control factor of the splitter length L/D ($D$is the diameter of the cylinder) varies from 0 to 1.5, and the Reynolds number ReD is considered to be 2400 and 3000. The experimental results show that the splitter plate has an effect on the stability of the wake turbulence in the closed channel. For the case of shorter splitter plate lengths ofL/D 0.5 and 0.75, compared with the case of a bare cylinder, the flow structure is significantly changed and the frequency of vortex shedding is reduced. For longer splitter lengths of $L/D = 1, 1.25$, and 1.5, the generation of secondary vortices is observed based on the proper orthogonal decomposition analysis of the snapshot. In addition, the turbulence characteristics correspond to the turbulent kinetic energy (TKE) and Reynolds shear stress correlation with the lowest value, the main vortex shedding frequency disappears. When $L/D = 1$, the splitter plate length has an optimal value to suppress speed fluctuations. In addition, the stabilizing effect of the splitter plate is more obvious when $Re = 3000$ Reynolds number than$Re = 2400$.

J. He et al(2018) [14]used the hybrid RANS-LES turbulence modeling method to simulate and physically analyze the turbulence flow around a cylinder at$Re = 3900$. Numerical research is carried out by using naoe-FOAM-SJTU, which is a viscous flow solver (naoe-FOAM-SJTU), which is developed based on the popular open source toolbox OpenFOAM. In order to simulate large separated flows at high Reynolds numbers, turbulence closure was selected as an improved

delayed separation eddy current simulation (IDDES) based on shear stress transfer (SST). In this study, the benefits of these hybrid methods in capturing eddy dynamics and frequency patterns are discussed. The drag coefficientCd and Strouhal number (St) were analyzed and compared with the experimental results. At the same time, the boundary layer transition phenomenon and flow characteristics are predicted more accurately.

M.Kaur and P.Kumar (2018) [15] they have numerically investigates the three-dimensional fluid flow with emphasis on the cylinder and wall gap effect. The non-dimensional gap ratio ($^{G}/_{D}$), between the cylinder end and the wall, ranges from 0, 2.5, 5, and 7.5 for the Reynolds number $3.7 * 10^{4}$. The reduction in the vortex shedding and increase in amplitude of frequency of the lift coefficient is observed with the reduction in the gap ratio. Thus, the coefficients of drag and lift show the effect of the gap ratio on the fluid structure in wake.

Z.Rahmani et al (2019) [16] Studied the behavior of a turbulent flowincompressible around cylindrical obstacles and explained the physical phenomena that occur in certain configurations. The flow is studied by the RANS method using the $k - \omega - SST$ turbulence model, and the Code_Saturne computer code is used to solve the equations that control the flow.After studying the case of a single cylinder as a verification case with a Reynolds number of 3900, the second part involves a square arrangement of four cylinders, the spacing between the cylinder centers is $^{P}/_{D} = 1.5$and the Reynolds number is equal to 3000.

X. Sun et al (2020) [17] Conducted a numerical study of flow-induced vibration (FIV) on a cylinder with an additional splitter plate in a laminar flow with $Re = 100$. First, a mechanical model and mathematical formula are proposed to describe the fluid-structure interaction (FSI) between the elastically supported cylinder-plate and the surrounding flow. Subsequently, the FSI solver was developed based on the feature-based splitting finite element method, and its accuracy and stability were verified using the vortex-induced vibration (VIV) of a plane cylinder with a reference solution. Finally, using FSI simulations, the effects of plate length (L), reduced speed, mass ratio, and damping coefficient on the dynamic response, fluid load and flow pattern of the cylinder-plate assembly were studied in detail. The length of the Ace board is increased from $^{L}/_{D} = 0\ to\ 1.5$ (D is the diameter of the cylinder).

CHAPTER 2: TURBULENCE MODELING

Introduction

In this chapter, we provide a definition of turbulence and computational fluid dynamics. We discussed some of the modeling methods used on CFD, also we mentioned turbulence models such as $(k-\varepsilon, k-\omega, and\ k-\omega-sst)$. The Navier-Stokes equations for controlling turbulence are given

2.1. Turbulence

Turbulence is arguably the most challenging area in fluid dynamics and the most limiting factor in accurate computer simulation of engineering flows. It is a classic multi-scale problem, well beyond human intuitive understanding and beyond the solving capabilities of even the most powerful modern parallel computers (for any foreseeable future). Turbulence has been described by Nobel Prize-winning physicist Richard Feynman as the "most important unsolved problem in classical physics." An even more pronounced quote is associated with Werner Heisenberg: “When I meet God, I will ask him two questions: Why relativity? And why the turbulence? I really think he will have an answer for the first. "***[18]***

Due to the technical importance of turbulence, models based on the correlation of individual experimental data have to a large extent been developed. The task of developing a general model of turbulence is difficult because turbulence occurs almost everywhere: Flows in rivers, oceans and the atmosphere are large-scale examples. Flows in pipes, pumps, turbines, combustion processes, in the wake of cars, planes and trains are just some technical examples. Even the blood flow in the aorta can be turbulent. In fact, it can be said that turbulence is a general type of medium and large scale flow, while laminar flows appear on a small scale and where the viscosity is high. For example, the flow of lubricating oils in bearings is laminar. ***[19]***

Fig.2.1: Turbulence from aircraft swirling clouds [20].

2.1.1. Characteristics of turbulence[21]

- The randomness or irregular nature of turbulent flows makes a solely deterministic approach to the turbulence problem impossible. Therefore, one must rely on statistical or conditional methods
- The large diffusive nature of turbulence causes rapid mixing & increased rates of mass, momentum and energy transfer.
- Turbulent flows always occur at high Re (i.e., inertia or non-linear) forces dominate the viscous forces.
- Turbulence is a continuum phenomenon governed by the equations of fluid mechanics. Even the smallest scales of motion occurring in a turbulent flow are larger than any molecular length scale.
- Turbulence is rotational, three-dimensional, and characterized by high levels of fluctuating vorticity. These random vorticity fluctuations which characterize turbulence could not maintain themselves if the velocity fluctuations were two-dimensional.
- All turbulent flows are dissipative. Viscous shear stresses perform deformation work, which increase the internal energy of the fluid (increased temperature) at the expense of the kinetic energy of the turbulence.

2.2. Computational Fluid Dynamics[22] [24]

Computational fluid dynamics (CFD) is a branch of fluid dynamics that provides a cost-effective way to analyze systems involving fluid flow, heat transfer, and related phenomena (such as chemical reactions) through computer-based simulation. The technology is very powerful and covers a wide range of industrial and non-industrial applications. Some examples are:

- aerodynamics of aircraft and vehicles: lift and drag
- hydrodynamics of ships
- power plant: combustion in internal combustion engines and gas turbines
- turbomachinery: flows inside rotating passages, diffusers etc.
- electrical and electronic engineering: cooling of equipment including microcircuits
- chemical process engineering: mixing and separation, polymer moulding
- external and internal environment of buildings: wind loading and heating/ventilation
- marine engineering: loads on off-shore structures
- environmental engineering: distribution of pollutants and effluents
- hydrology and oceanography: flows in rivers, estuaries, oceans
- meteorology: weather prediction
- biomedical engineering: blood flows through arteries and veins

Fig.2.2: CFD Simulation of a cyclist [23].

Computational Fluid Dynamics (CFD) provides a qualitative (and sometimes even quantitative) prediction of fluid flows by means of:

- Mathematical modelling (partial differential equations)
- Numerical methods (discretization and solution techniques)
- Software tools (solvers, pre- and post-processing utilities) CFD enables scientists and engineers to perform "numerical experiments" (i.e. computer simulations) in a 'virtual flow laboratory.

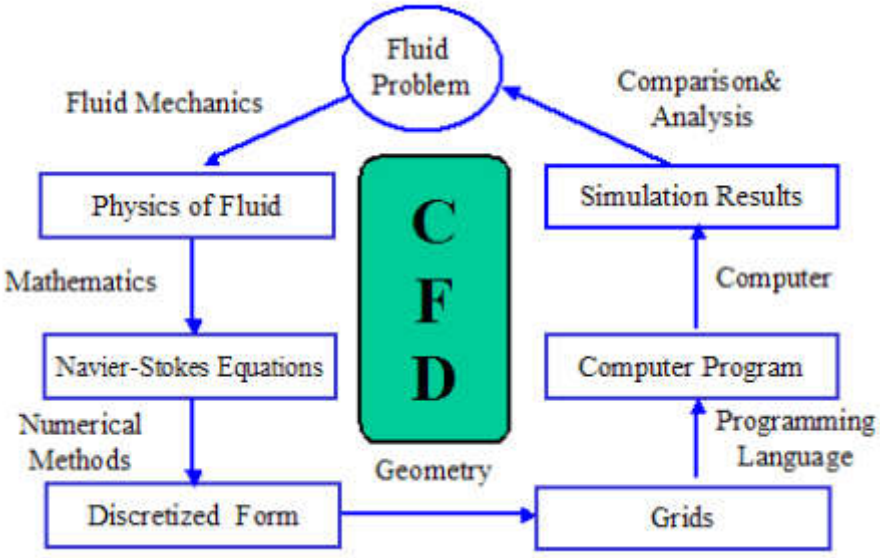

Fig2.3: Process of Computational Fluid dynamics [24].

2.3. Equations ofNavier-Stokes

The Navier-Stokes equations are nonlinear partial differential equations that describe the motion of fluids in the continuous media approximation.

Applying the mass, momentum and energy conservation,we can derive the continuity equation, the momentum equation, and the energy equation as follows. **[25]**

Continuity equation

$$\frac{D\rho}{Dt} + \frac{\partial U_i}{\partial x_i} = 0 \tag{2.1}$$

Momentum Equation

$$\underbrace{\rho \frac{\partial U_j}{\partial t}}_{\text{I}} + \underbrace{U_i \frac{\partial U_j}{\partial x_i}}_{\text{II}} = \underbrace{-\frac{\partial P}{\partial x_j}}_{\text{III}} \underbrace{-\frac{\partial \tau_{ij}}{\partial x_i}}_{\text{IV}} + \underbrace{\rho g_j}_{\text{V}} \tag{2.2}$$

Where

$$\tau_{ij} = -\mu\left(\frac{\partial U_j}{\partial x_i} + \frac{\partial U_i}{\partial x_j}\right) + \frac{2}{3}\delta_{ij}\mu\frac{\partial U_k}{\partial x_k} \tag{2.3}$$

I: Local change with time

II: Momentum convection

III: Surface force

IV: Molecular-dependent momentum exchange (diffusion)

V: Mass force

2.3.1. Energy Equation

$$\underbrace{\rho c_\mu \frac{\partial T}{\partial t}}_{\text{I}} + \underbrace{\rho c_\mu U_i \frac{\partial T}{\partial x_i}}_{\text{II}} = \underbrace{-P\frac{\partial U_i}{\partial x_i}}_{\text{III}} + \underbrace{\lambda \frac{\partial^2 T}{\partial {x_i}^2}}_{\text{IV}} - \underbrace{\tau_{ij}\frac{\partial U_j}{\partial x_i}}_{\text{V}} \tag{2.4}$$

I: Local energy change with time

II: Convective term

III: Pressure work

IV: Heat flux (diffusion)

V: Irreversible transfer of mechanical energy into heat

If the fluid is compressible, we can simplify the continuity equation and momentum equation asfollows.

Continuity Equation

$$\frac{\partial U_i}{\partial x_i} = 0 \qquad (2.5)$$

Momentum Equation

$$\rho \frac{\partial U_j}{\partial t} + \rho U_i \frac{\partial U_j}{\partial x_i} = -\frac{\partial P}{\partial x_j} - \mu \frac{\partial^2 U_j}{\partial {x_i}^2} + \rho g_j \qquad (2.6)$$

2.4. Modeling Methods[26]

Since engineering flows are mostly turbulent in nature when dealing with CFD simulations, we have to solve turbulent flows most of the time. Turbulence modeling is one of the most important aspects of CFD modeling, and correct turbulence modeling is critical to obtaining correct and reliable CFD results.

The figure below summarizes the most common approaches to solving turbulent flows. The computational cost of CFD simulations increases from RANS to DNS as the number of degrees of freedom required to solve the flow increases. A consequence of computational costs is that scale-resolution methods such as DNS and LES are typically applied to simple geometries and academic setups, while hybrid RANS-LES, URANS, and RANS can be applied to complex industrial problems.

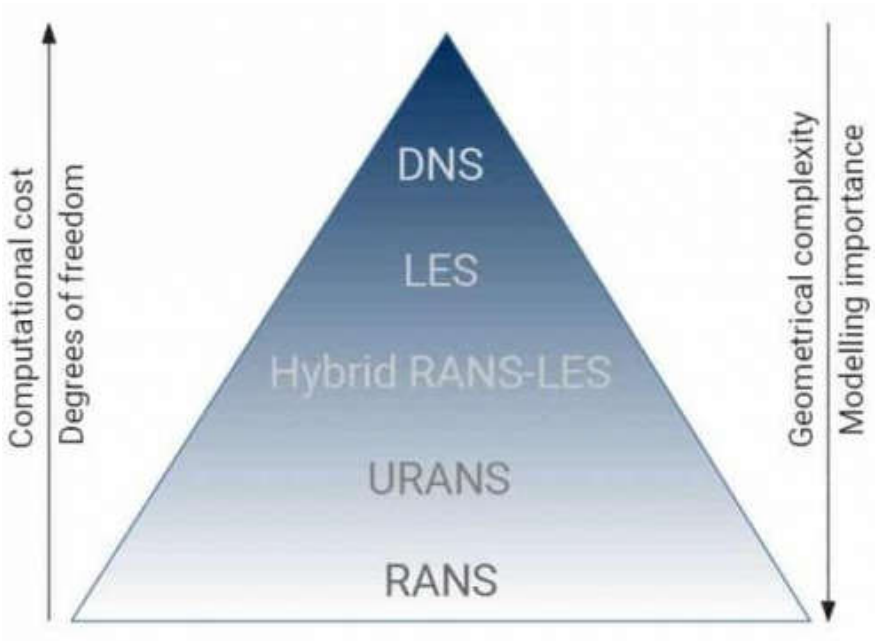

***Fig.2.4: Turbulence models in CFD from RANS to DNS.*[26]**

2.4.1. Reynolds Averaged Navier-Stokes (RANS)

Reynolds Averaged Navier-Stokes Equations (RANS): A statistical treatment is applied to the Navier-Stokes equations which are then solved to provide average quantities (see figure2.5)

directly. By doing so, small scales are not present in the equations and the numerical method and mesh requirement are less demanding.*[27]*

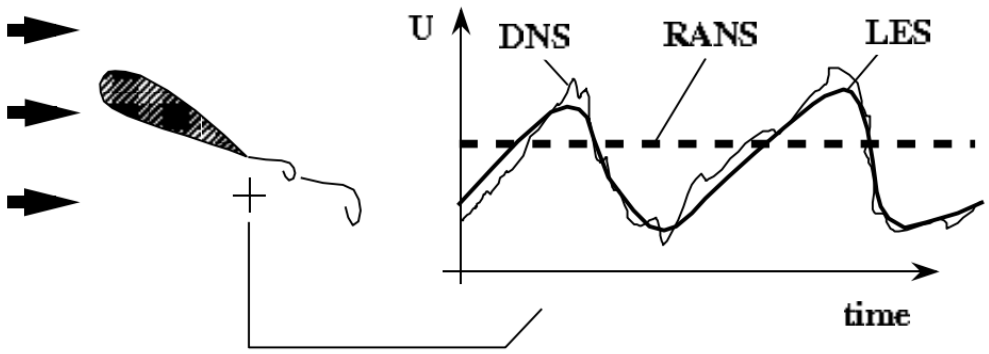

Fig2.5: Principle of the DNS, RANS and LES approaches.[27]

This is the most widely used method in the modern design chain to reduce the number of experimental tests. The price to pay is the need to model the correlations that appear when averaging the nonlinear terms of the basic equations. RANS modeling is the most common and widespread approach in industrial applications. If the flow of interest is characterized by moving parts or a periodic flow characteristic, these can be solved using unstable RANS (URANS).

All RANS models have some limitations due to the modeling assumptions used to derive the mathematical formulation of the model. For certain applications, it might be required to use more detailed approaches that instead of modeling all of the turbulence scales, try to resolve the most energy containing structures of the flow. This approach is called Large Eddy Simulations (LES).**[26]**

2.4.2. Large Eddy Simulation (LES).[28]

Large eddy simulation (LES) is an intermediate technique between the direct simulation of turbulent flows and the solution of Reynolds averaged equations. In LES, the contribution of large energy transfer structures to momentum and energy transfer is accurately calculated and only the effect of the smallest scales of turbulence is modeled. As small scales appear to be more homogeneous and versatile, and less prone to boundary conditions than large scales, it is hoped that their models may be simpler and require fewer adjustments when applied to different flows than similar models for the RANS equation.

Early LES applications were limited to "building-block" flows: homogeneous turbulence, free shear flows, flows in flat channels. With the introduction of new models that made it possible to perform more accurate calculations with less empiricism than before, the LES is now used not only to calculate standard, well-documented test cases, but also to study the physical phenomena found in more complex, engineering-like applications**.**

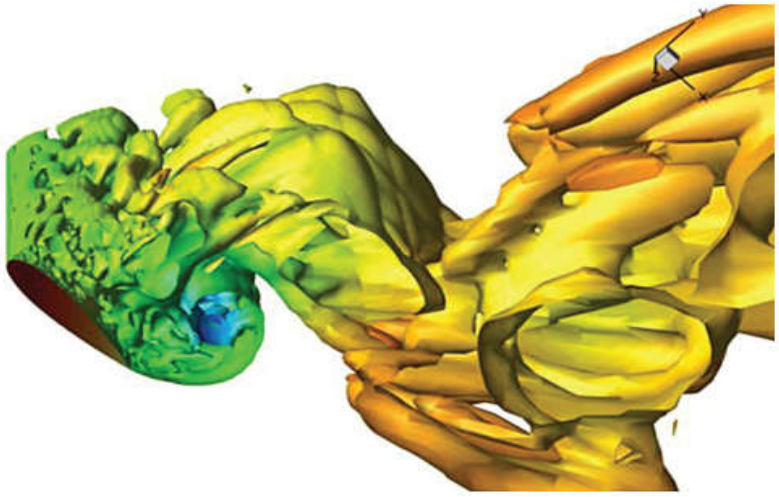

Fig2.6: LES simulation of a wing with wide angle of attack.[29]

2.4.3. Hybrid RANS-LES model (DES) *[26]*

There are a series of turbulence models that can take advantage of LES modeling while retaining the efficiency of the RANS model, in which LES is too expensive. These go under the name of hybrid RANS-LES models.

Most mesh resolutions tend to be located near surfaces and objects of interest, as in LES, the flow needs to be fully resolved near the walls. Therefore, if the restriction on the increase in resolution close to the wall can be relaxed, the cost of the LES can be greatly reduced. One of the most common hybrid methods uses LES modeling away from the wall and RANS modeling close to the wall. This method is called Detached Eddy Simulation (DES).The DES approach is becoming very popular in industrial applications as it helps overcoming some of the limitations of the RANS models as well as offering increased insight in the solution as the simulation is always run as unsteady flow, even for cases that have a steady state solution, and the finer spatial resolution allows to study detailed behaviour of the flow of interest. All of it at a reduced cost compared to a fully fledged LES approach.

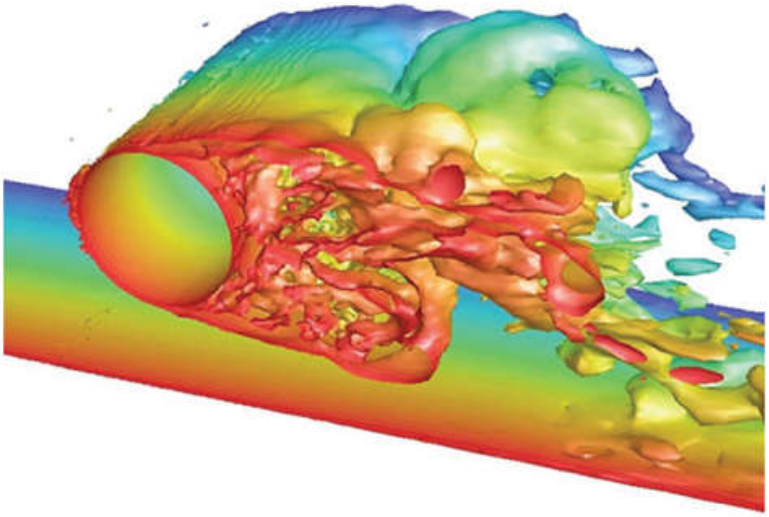

Fig2.7:DES simulation of a cylinder above a surface.[29]

2.4.4. Direct Numerical Simulation (DNS)

Direct numerical simulation (DNS) is the most accurate method of solving turbulence in fluids. In DNS the Navier-Stokes equations are solved on a fine mesh to resolve all the spatial and temporal scales present in the flow. In order to ensure high accuracy of the discrete solution, schemes with low numerical errors are necessary. Spectral methods with their low dissipation and dispersion errors are very attractive in this regard. Since their inception in early 1970's, spectral methods have been routinely applied towards direct simulation of turbulent flows. Some of the earliest applications were in isotropic turbulence using Fourier series based methods. As the community turned its attention to solving practical flows, the need for schemes that are efficient in handling complex geometries arose. This led to the development of spectral element methods. [30]

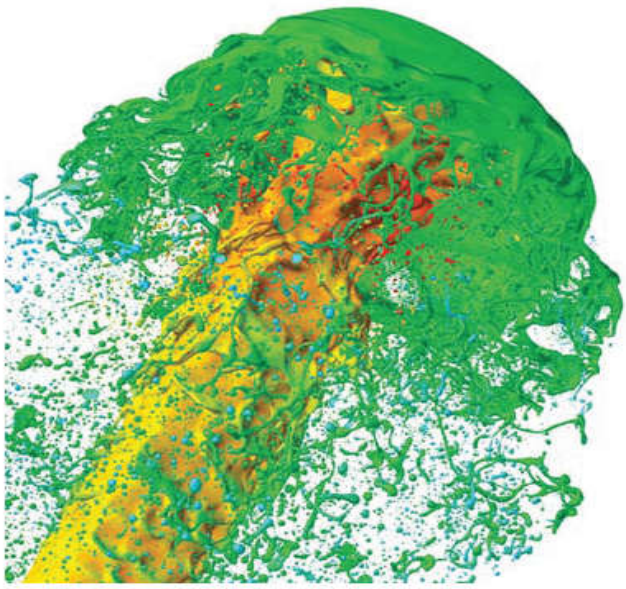

Fig2.8: DNS simulation of a liquid jet [31]

2.5. Turbulence model

2.5.1. $k-\varepsilon$ Model*[32]*

So far, until the last decade of the 20th century, the most popular two-equation model is the $k-\varepsilon$ model. The earliest development work based on this model was the work of Chou (1945), Davidov (1961) and Harlow and Nakayama (1968). The widespread use of this model began with the version introduced by Jones and Launder (1972). Launder and Sharma (1974) then "re-adjusted" the closure coefficient of the model, creating a model commonly referred to as the standard $k-\varepsilon$ model.

The quantity ε is the dissipation per unit mass and is defined by the following correlation.

$$\varepsilon = \nu \overline{\frac{\partial u_i'}{\partial x_k}\frac{\partial u_i'}{\partial x_k}} \tag{2.7}$$

We begin with Equation (2.8)

$$\frac{\partial k}{\partial t} + U_j\frac{\partial k}{\partial x_j} = \tau_{ij}\frac{\partial U_i}{\partial x_j} - \varepsilon + \frac{\partial}{\partial x_j}\left[(\nu + \nu_T/\sigma_k)\frac{\partial k}{\partial x_j}\right] \tag{2.8}$$

Where τ_{ij} is Reynolds-stress tensor

$$\tau_{ij} = 2\nu_T S_{ij} - \frac{2}{3}k\delta_{ij} \tag{2.9}$$

The exact equation for ε is derived by taking the following moment of the Navier-Stokes equation:

$$\varepsilon = \nu \overline{\frac{\partial u_i'}{\partial x_j}\frac{\partial}{\partial x_j}[N(u_i)]} \tag{2.10}$$

Where $N(u_i)$ is the Navier-Stokes operator

$$N(u_i) = \rho\frac{\partial u_i}{\partial t} + \rho u_k\frac{\partial u_i}{\partial x_k} + \frac{\partial p}{\partial x_i} - \mu\frac{\partial^2 u_i}{\partial x_k \partial x_k} \tag{2.11}$$

After a considerable amount of algebra, the following exact equation for ε results.

$$\frac{\partial \varepsilon}{\partial t} + U_i\frac{\partial \varepsilon}{\partial x_j} = -2\nu\left[\overline{u_{\iota,k}'u_{J,k}'} + \overline{u_{k,\iota}'u_{k,J}'}\right]\frac{\partial U_i}{\partial x_j} - 2\nu\,\overline{u_k'u_{\iota,J}'}\frac{\partial^2 U_i}{\partial x_k \partial x_j} - 2\nu\,\overline{u_{\iota,k}'u_{\iota,m}'u'_{k,m}}$$
$$- 2\nu^2\overline{u_{\iota,km}'u_{\iota,km}'} + \frac{\partial y}{\partial x}\left[\nu\frac{\partial y}{\partial x} - \nu\overline{u'_J u'_{\iota,m}u'_{\iota,m}} - 2\frac{\nu}{\rho}\overline{p'_{,m}u'_{J,m}}\right] \tag{2.12}$$

The exact transport equation of ε is too complex to be exploited in a simple model. It is for this reason that authors like Harlow and Nakayama (1968) and Hanjalic (1970) have proposed a simplified equation, assuming that the structure of this equation is similar to that of k: convection - source - sink - viscous and turbulent diffusions ***[28]***. The standard k-ε is as follows:

2.5.1.1. Kinematic Eddy Viscosity:

$$\nu_T = {C_\mu k^2}/{\varepsilon} \qquad (2.13)$$

2.5.1.2. Turbulence Kinetic Energy:

$$\frac{\partial k}{\partial t} + U_j \frac{\partial k}{\partial x_j} = \tau_{ij} \frac{\partial U_i}{\partial x_j} - \varepsilon + \frac{\partial}{\partial x_j}\left[(\nu + \nu_T/\sigma_k)\frac{\partial k}{\partial x_j}\right] (2.14)$$

2.5.1.3. Dissipation Rate:

$$\frac{\partial \varepsilon}{\partial t} + U_j \frac{\partial \varepsilon}{\partial x_j} = C_{\varepsilon 1} \frac{\varepsilon}{k} \tau_{ij} \frac{\partial U_i}{\partial x_j} - C_{\varepsilon 2} \frac{\varepsilon^2}{k} + \frac{\partial}{\partial x_j}\left[(\nu + \nu_T/\sigma_\varepsilon)\frac{\partial \varepsilon}{\partial x_j}\right] (2.15)$$

2.5.1.4. Closure Coefficients and Auxiliary Relations:

$$C_{\varepsilon 1} = 1.44, \quad C_{\varepsilon 2} = 1.92, \quad C_\mu = 0.09, \quad \sigma_k = 1.0, \quad \sigma_\varepsilon = 1.3 \ (2.16)$$

$$\omega = {\varepsilon}/{C_\mu k} \ \ and \ \ \ell = {C_\mu k^{3/2}}/{\varepsilon} \qquad (2.17)$$

A more recent version of the $k-\varepsilon$ model has been developed by Yakhot and Orszag (1986) [see also Yakhot et al. (1992)]. Using techniques from renormal- ization group theory, they have developed what is known as the RNG $k-\varepsilon$ model. The eddy viscosity, k *and* ε are still given by Equations (2.13), (2.14) and (2.15). However, the model us a modified coefficient, $C_{\varepsilon 2}$, defined by

$$C_{\varepsilon 2} \equiv \tilde{C}_{\varepsilon 2} + \frac{C_\mu \lambda^3 (1 - \lambda/\lambda_0)}{1 + \beta \lambda^3}, \qquad \lambda \equiv \frac{k}{\varepsilon}\sqrt{2 S_{ij} S_{ji}} \ (2.18)$$

The closure coefficients for the RNG $k-\varepsilon$ model are

$$C_{\varepsilon 1} = 1.42, \quad \tilde{C}_{\varepsilon 2} = 1.68, \quad C_\mu = 0.058, \quad \sigma_\varepsilon = 0.72, \quad \sigma_k = 0.72 \ (2.19)$$

$$\beta = 0.012, \quad \lambda_0 = 4.38 \qquad (2.20)$$

2.5.2. $k-\omega$ Model[32]

Kolmogorov (1942) proposed the first two-equation model turbulence. Kolmogorov chose the kinetic energy of the turbulence as one of turbulence parameters and, like Prandtl (1945), modeled the differential equation governing its behavior. His second parameter was the dissipation per unit turbulence kinetic energy, ω. In his $k-\omega$ model, ω satisfies a differential equation similar to the equation for k. With no prior knowledge of Kolmogorov's work, Saffman (1970) formulated a kw model that would prove superior to the Kolmogorov model. As part of the Imperial College efforts on two-equation models, Spalding offered an improved version of the Kolmogorov model that removed some of its flaws.

Shortly after formulation of Saffman's model and continuing to the present time, Wilcox et al. [Wilcox and Alber (1972), Saffman and Wilcox (1974), Wilcox and Traci (1976), Wilcox and Rubesin (1980), Wilcox (1988a) and Wilcox (1998)] have pursued further development and application of k-w turbulence models.

Kolmogorov's approach is to recognize that the number of physical processes normally observed in fluid motion is quite small. The most common processes are instability, convection (often called advection), diffusion, dissipation, dispersion, and generation. Combining physical reasoning and dimensional analysis, Kolmogorov assumed the following equation ω

$$\frac{\partial \omega}{\partial t}+U_j\frac{\partial \omega}{\partial x_j}=-\beta\omega^2+\frac{\partial}{\partial x_j}\left[\sigma\nu_T\frac{\partial \omega}{\partial x_j}\right] \qquad (2.21)$$

The following version of the k-w model dramatically improves predictive accuracy of the Wilcox (1988a) model for free shear flows and strongly separated flows

2.5.2.1. Kinematic Eddy Viscosity:

$$\nu_T=\frac{k}{\tilde{\omega}},\qquad \tilde{\omega}=max\left\{\omega,C_{lim}\sqrt{\frac{2S_{ij}S_{ij}}{\beta^*}}\right\},\qquad C_{lim}=\frac{7}{8} \quad (2.22)$$

2.5.2.2. Turbulence Kinetic Energy:

$$\frac{\partial k}{\partial t}+U_j\frac{\partial k}{\partial x_j}=\tau_{ij}\frac{\partial U_i}{\partial x_j}-\beta^*k\omega+\frac{\partial}{\partial x_j}\left[\left(\nu+\sigma^*\frac{k}{\omega}\right)\frac{\partial k}{\partial x_j}\right] \quad (2.23)$$

2.5.2.3. Specific Dissipation Rate:

$$\frac{\partial \omega}{\partial t}+U_j\frac{\partial \omega}{\partial x_j}=\alpha\frac{\omega}{k}\tau_{ij}\frac{\partial U_i}{\partial x_j}-\beta\omega^2+\frac{\sigma_d}{\omega}\frac{\partial k}{\partial x_j}\frac{\partial \omega}{\partial x_j}+\frac{\partial}{\partial x_j}\left[\left(\nu+\sigma\frac{k}{\omega}\right)\frac{\partial \omega}{\partial x_j}\right] \quad (2.24)$$

2.5.2.4. Closure Coefficients and Auxiliary Relations:

$$\alpha = \frac{13}{25}, \qquad \beta = \beta_0 f_\beta, \qquad \beta^* = \frac{9}{100}, \qquad \sigma = \frac{1}{2}, \qquad \sigma^* = \frac{3}{5}, \qquad \sigma_{do} = \frac{1}{8} \quad (2.25)$$

$$\sigma_d = \begin{cases} 0, & \frac{\partial k}{\partial x_j}\frac{\partial \omega}{\partial x_j} \leq 0 \\ \sigma_{do}, & \frac{\partial k}{\partial x_j}\frac{\partial \omega}{\partial x_j} > 0 \end{cases} \quad (2.26)$$

$$\beta_0 = 0.0708, \qquad f_\beta = \frac{1 + 85\chi_\omega}{1 + 100\chi_\omega}, \qquad \chi_\omega \equiv \left|\frac{\Omega_{ij}\Omega_{jk}S_{ki}}{(\beta^*\omega)^3}\right| \quad (2.27)$$

$$\varepsilon = \beta^*\omega k \qquad and \qquad \ell = {k^{1/2}}/{\omega} \quad (2.28)$$

We refer to Equations (2.22) – (2.28) as the Wilcox (2006) $k-\omega$ model.

The tensors Ω_{ij} and S_{ij}appearing in Equation (2.27) are the mean-rotation and mean-strain-rate tensors, respectively defined by

$$\Omega_{ij} = \frac{1}{2}\left(\frac{\partial U_i}{\partial x_j} - \frac{\partial U_j}{\partial x_i}\right), \qquad S_{ij} = \frac{1}{2}\left(\frac{\partial U_i}{\partial x_j} + \frac{\partial U_j}{\partial x_i}\right) \quad (2.29)$$

2.5.3.$k-\omega$ - SST Model

The $SST\ k-\omega$ turbulence model [Shear Stress Transport-Menter 1993] is a very popular two-equation eddy viscosity model. The shear stress transmission (SST) formula combines the advantages of both worlds. Using the $k-\omega$ formula inside the boundary layer allows the model to be used directly through the viscous sub-layer to the wall, so the $SST\ k-\omega$ model can be used as a Low-Re turbulence model without any additional damping function. The SST formula also switches to the $k-\varepsilon$ behavior in the free flow, thus avoiding the common $k-\omega$ problem that the model is too sensitive to the turbulence properties of the inlet free flow. Authors using the $SST\ k-\omega$ model are generally praised for their good behavior in adverse pressure gradients and separated flows. The $SST\ k-\omega$ model does produce excessive turbulence levels in areas with large normal strains (such as stagnant areas and areas with strong acceleration).This tendency is much less pronounced than with a normal k-ε model though.[33]

2.5.3.1. Kinematic Eddy Viscosity:

$$\nu_T = \frac{a_1 k}{max(a_1\omega, SF_2)} \quad (2.30)$$

$\boldsymbol{F_2}$ (Second blending function)

$$F_2 = tanh\left[\left[\max\left(\frac{2\sqrt{k}}{\beta^*\omega y}, \frac{500\nu}{y^2\omega}\right)\right]^2\right] \quad (2.31)$$

2.5.3.2. Turbulence Kinetic Energy:

$$\frac{\partial k}{\partial t} + U_j\frac{\partial k}{\partial x_j} = P_k - \beta^* k\omega + \frac{\partial}{\partial x_j}\left[(\nu + \sigma_k\nu_T)\frac{\partial k}{\partial x_j}\right] \quad (2.32)$$

$\boldsymbol{P_k}$ (Production limiter)

$$P_k = min\left(\tau_{ij}\frac{\partial U_i}{\partial x_j}, 10\beta^* k\omega\right) \quad (2.33)$$

2.5.3.3. Specific Dissipation Rate:

$$\frac{\partial \omega}{\partial t} + U_j\frac{\partial \omega}{\partial x_j} = \alpha S^2 - \beta\omega^2 + \frac{\partial y}{\partial x}\left[(\nu + \sigma_\omega\nu_T)\frac{\partial \omega}{\partial x_j}\right] + 2(1 - F_1)\sigma_{\omega^2}\frac{1}{\omega}\frac{\partial k}{\partial x_i}\frac{\partial \omega}{\partial x_i} \quad (2.34)$$

$\boldsymbol{F_1}$ (Blending Function)

$$F_1 = tanh\left\{\left\{min\left[max\left(\frac{\sqrt{k}}{\beta^*\omega y}, \frac{500\nu}{y^2\omega}\right), \frac{4\sigma_{\omega^2}k}{CD_{k\omega}y^2}\right]\right\}^2\right\} \quad (2.35)$$

Where $CD_{k\omega}$ define by

$$CD_{k\omega} = max\left(2\rho\sigma_{\omega 2}\frac{1}{\omega}\frac{\partial k}{\partial x_i}\frac{\partial \omega}{\partial x_i}, 10^{-10}\right) \quad (2.36)$$

***Note**: $F_1 = 1$ inside the boundary layer and 0 in the free stream. And y is the closest distanceto the wall.*

2.5.3.4. Closure Coefficients and Auxiliary Relations:

All constants are calculated by mixing the corresponding constants of the model k - ε andmodel k - $\omega$by:

$$\alpha = \alpha_1 F_1 + \alpha_2(1 - F_1) \quad (2.37)$$

$$\alpha_1 = \frac{5}{9}, \quad \alpha_2 = 0.44, \quad \beta_1 = \frac{3}{40}, \quad \beta_2 = 0.0828, \quad \beta^* = \frac{9}{100} \quad (2.38)$$

$$\sigma_{k1} = 0.85,\ \sigma_{k2} = 1,\ \sigma_{\omega 1} = 0.5,\ \sigma_{\omega 2} = 0.856 \quad (2.39)\textbf{[14]}$$

CHAPTER 3: NUMERICAL RESOLUTION AND FREE SOFTWARES

Introduction

In the following, we will introduce the open source and free CFD softwares and its advantages and how it works in numerical calculations (Code_Saturn, GMSH, EnSight and Paraview). We present also the free software Grace, which is a 2D graphics drawing tool.

3.1. Presentation of GMSH

Gmsh is an open source 3D finite element mesh generator with a built-in CAD engine and post-processor, developed by Christophe Geuzaine and Jean-François Remacle.Its design goal is to provide a fast, light and user-friendly meshing tool with parametric input and advanced visualization capabilities. Gmsh is built around four modules: geometry, mesh, solver, and post-processing. The specification of any input of these modules is done interactively using a graphical user interface, in an ASCII text file using Gmsh's own scripting language (.geo file) [34].

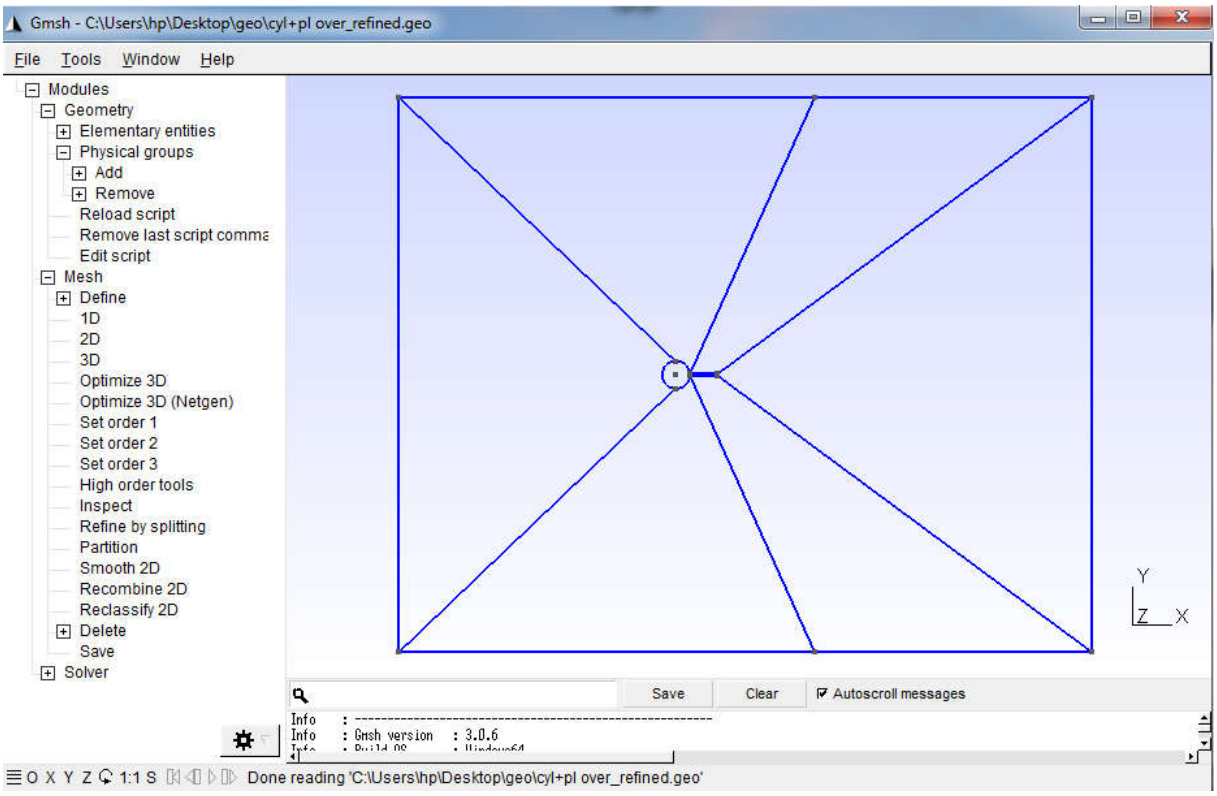

Fig.3.1: Gmsh graphical interface.

3.2. Code_Saturne Software

Code_Saturne is the **free**, **open-source** software developed and released by EDF to solve computational fluid dynamics (CFD) applications.

It solves the Navier-Stokes equations for 2D, 2D-axisymmetric and 3D flows, steady or unsteady, laminar or turbulent, incompressible or weakly dilatable, isothermal or not, with scalars transport if required.

Several turbulence models are available, from Reynolds-Averaged models to Large-Eddy Simulation models. In addition, a number of specific physical models are also available as modules: gas, coal and heavy-fuel oil combustion, semi-transparent radiative transfer, particle-tracking with Lagrangian modeling, Joule effect, electrics arcs, weakly compressible flows, atmospheric flows, rotor/stator interaction for hydraulic machines.[35]

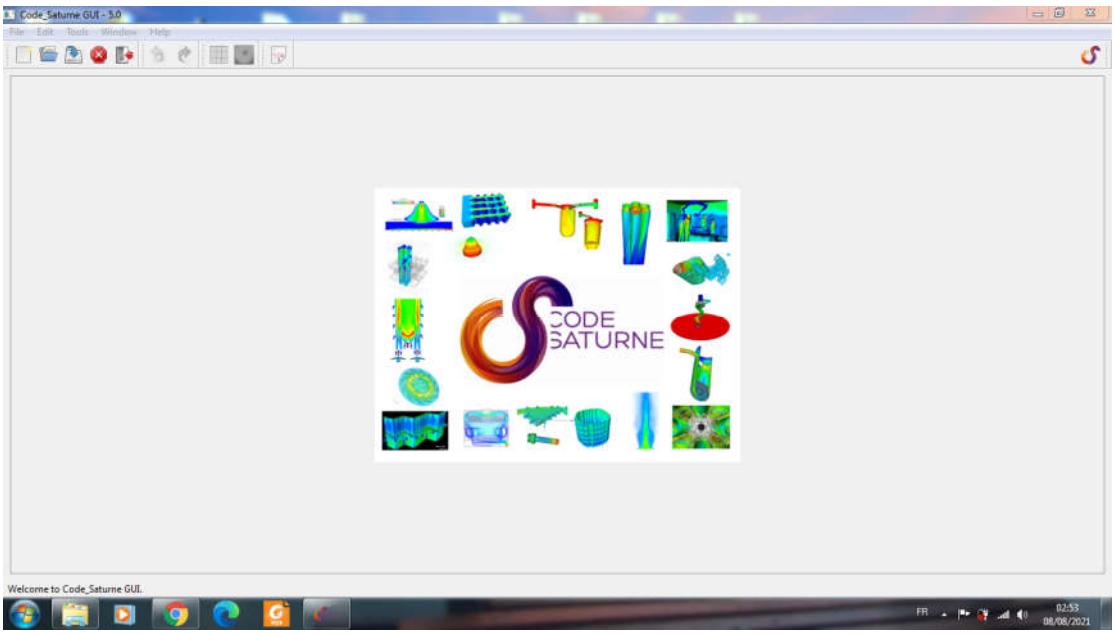

*Fig.3.2-**Code_Satunre graphical interface***

3.2.1. Numerical method[37]

3.2.1.1. Discretization

*Code_Saturne*is based on a co-located Finite Volume approach that handles meshes with any type of cell (tetrahedral, hexahedral, prismatic, pyramidal, polyhedral…) and any type of grid structure (unstructured, block structured, hybrid, conforming or with hanging nodes…).

*Code_Saturne*can solve flows in steady or unsteady mode. It uses a theta scheme for the time discretization.

3.2.1.2. Velocity-pressure coupling

*Code_Saturne*uses a fractional step method, similar to SIMPLEC.

1. Velocity prediction: Solve the momentum equation with an explicit pressure gradient and obtain a predicted velocity

2. Pressure correction: Use the continuity equation to enforce mass conservation
3. Update velocity field using ∇ P

After the velocity has been updated, the resolution of turbulent variables and scalars is done according to their time scheme.

Rhie& Chow interpolation is used when solving the pressure to avoid oscillations.

3.2.1.3. Linear system resolution

*Code_Saturne*has different ways of solving the linear system:

- Jacobi (default for velocity, temperature, turbulent variables, passive scalars)
- Algebraic multigrid (default for pressure)
- Conjugate gradient
- Stabilized bi-conjugate gradient (BI-CGSTAB)

3.2.1.4. Convective scheme

Different schemes for convective terms are available in *Code_Saturne*:

- First order Upwind Scheme
- Centered scheme
- Second Order Linear Upwind (SOLU) Scheme
- Blended scheme between upwind and second order scheme

A slope test is activated by default for second order schemes to switch from second order to upwind in case of overshoots

3.2.1.5. Gradient calculation

In *Code_Saturne*several options are available:

- Iterative reconstruction of the non-orthogonalities (initialization by zero or based on the least-square method)
- Least squares method (with a standard, extended or partial extended neighborhood)

3.3. EnSight Software

EnSight is a 3-D post-processing and visualization software program to analyze, visualize and communicate your simulation and experimental data, developed by CEI Inc.[36]

EnSight is a data fusion program. It consolidates data from multiple engineering simulations and other sources to help explore and explain complex systems and processes. It handles simulation data from a wide range of physics from fluids, structures, particles, crash, electromagnetic and more. And it imports data from experiments, wind tunnels, imaging systems like MRI, and images and animations. With EnSight, you can create and communicate the best looking, clear, highest resolution simulation results on datasets that were previously thought to be too big to handle.

EnSight is a general purpose post processor that can visualize simulation data from ANSYS and most other CFD, FEA collision, electromagnetic, DEM, rigid body solutions. [37]

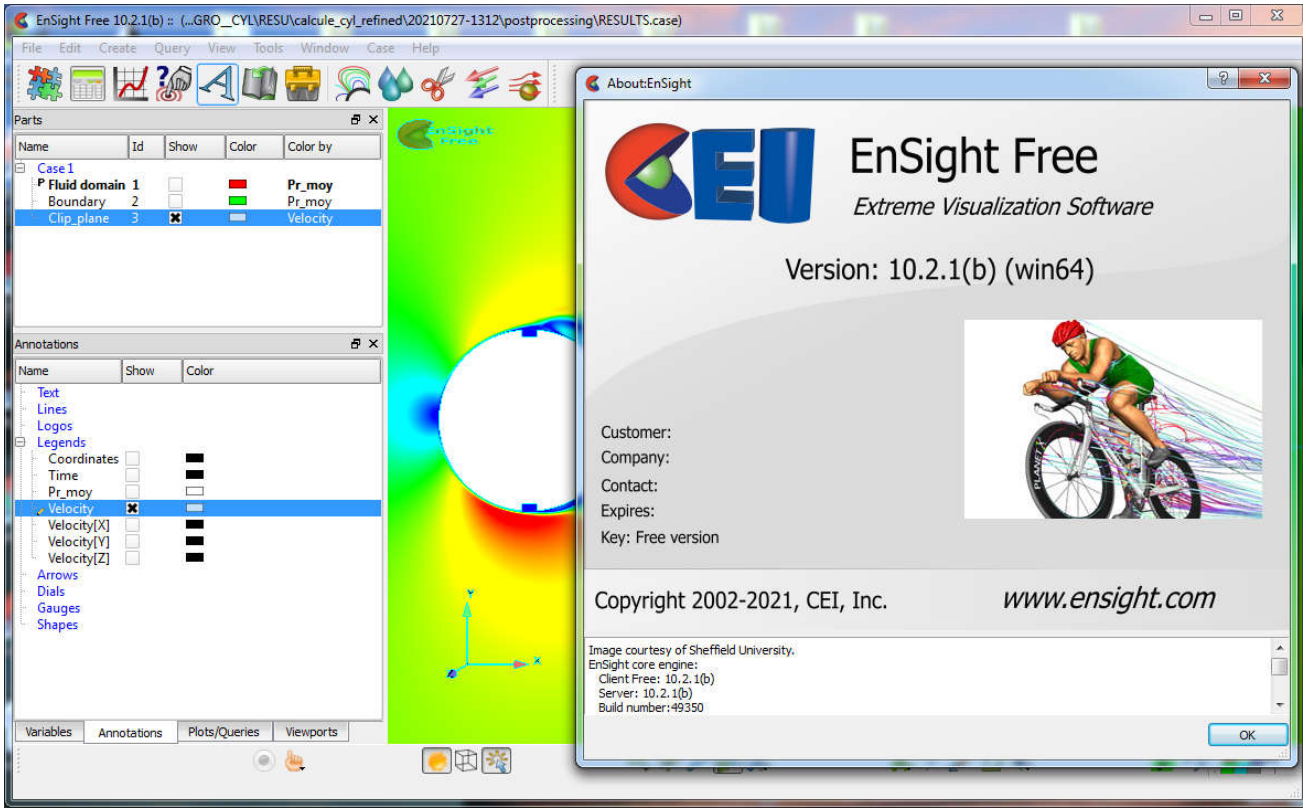

Fig.3.3: Ensight graphical interface

3.4. Presentation of Paraview

ParaView is an open source multi-platform application designed to visualize data sets of different sizes from small to large. The goals of the ParaView project include the development of open source, multi-platform visualization applications that support distributed computing models to process large data sets. It has an open, flexible and intuitive user interface. In addition, ParaView is built on an extensible architecture based on open standards. ParaView runs on distributed and shared memory parallel and single-processor systems, and has been successfully tested on Windows, Linux, Mac OS X, IBM Blue Gene, Cray XT3 and various Unix workstations and

clusters. At the bottom, ParaView uses a visualization toolkit as a data processing and rendering engine, and has a user interface written using the Qt cross-platform application framework.***[38]***

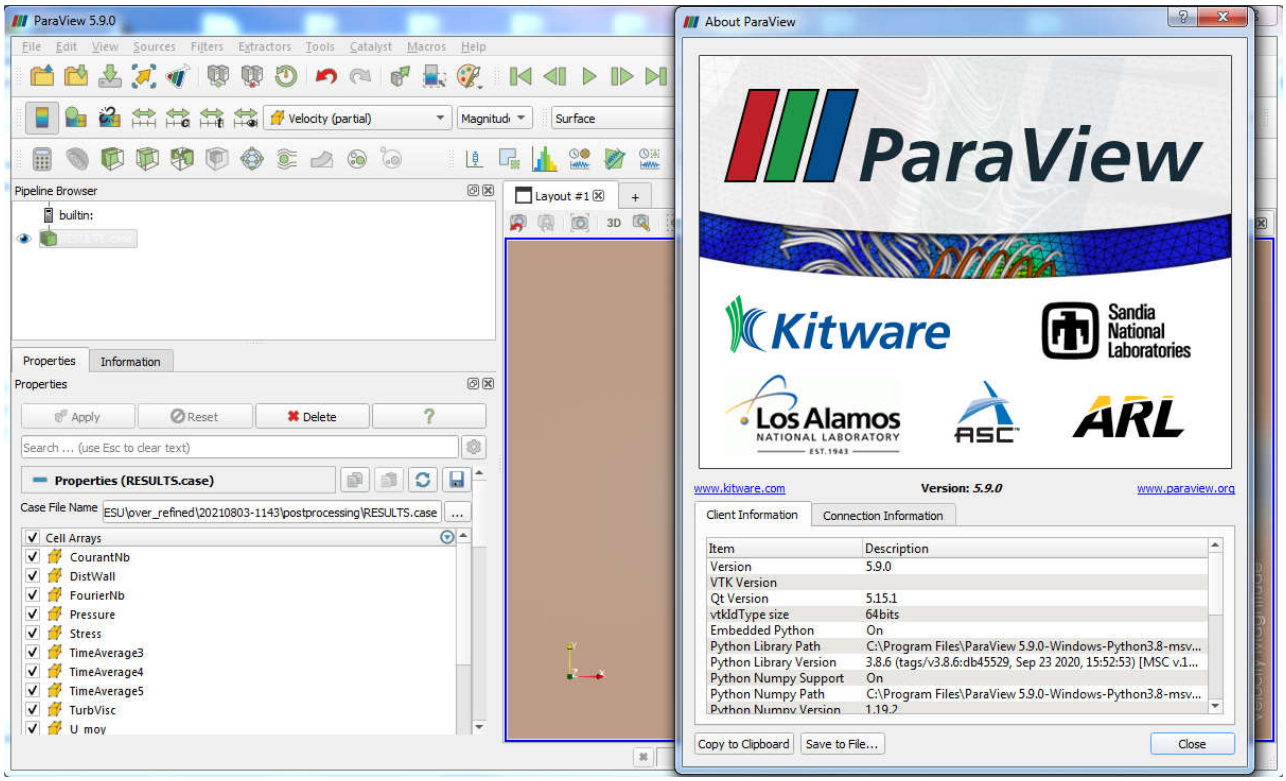

Fig.3.4: paraview graphical interface

ParaView leverages parallel data processing and rendering to enable interactive visualization for extremely large datasets. It also includes support for large displays including tiled displays and immersive 3D displays with head tracking and wand control capabilities.

ParaView also supports scripting and batch processing using Python. Using included Python modules, you can write scripts that can perform almost all the functionality exposed by the interactive application and much more.

ParaView is open-source (BSD licensed, commercial software friendly). As with any successful open-source project, ParaView is supported by an active user and developer community.[39]

3.4.1 Basics of visualization in ParaView

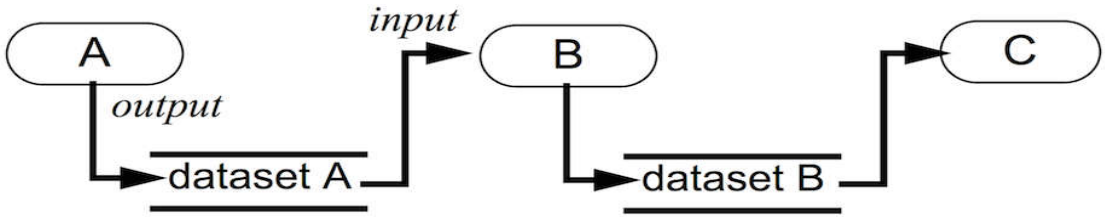

Fig.3.5. Visualization model: Process objects A, B, and C input and/or output one or more data objects.

Data objects represent and provide access to data; process objects operate on the data. Objects A, B, and C are source, filter, and mapper objects, respectively.

Visualization is the process of converting raw data into images and renderings to gain a better cognitive understanding of the data. **ParaView** uses VTK, the Visualization Toolkit, to provide the backbone for visualization and data processing.

3.5 Grace software

Grace is a tool for making two-dimensional graphs of numerical data. It uses X11 and M*tif to run under various (if not all) UNIX styles. Its functions are roughly similar to GUI-based programs such as Sigmaplot or Microcal Origin, and script-based tools such as gnuplot or Genplot. Its advantage is that it combines the convenience of a graphical user interface with the powerful functions of a scripting language, enabling it to perform complex calculations or perform automated tasks.

Grace is derived from Xmgr (aka ACE/gr) and was originally written by Paul Turner.
Starting from version 4.00, under the coordination of EvgenyStambulchik, a team of volunteers took over the development work.
When its copyright was changed to GPL, its name was changed to Grace, which stands for "GRaphing, Advanced Computation and Exploration of data" or "Grace Revamps ACE/gr".**[40]**

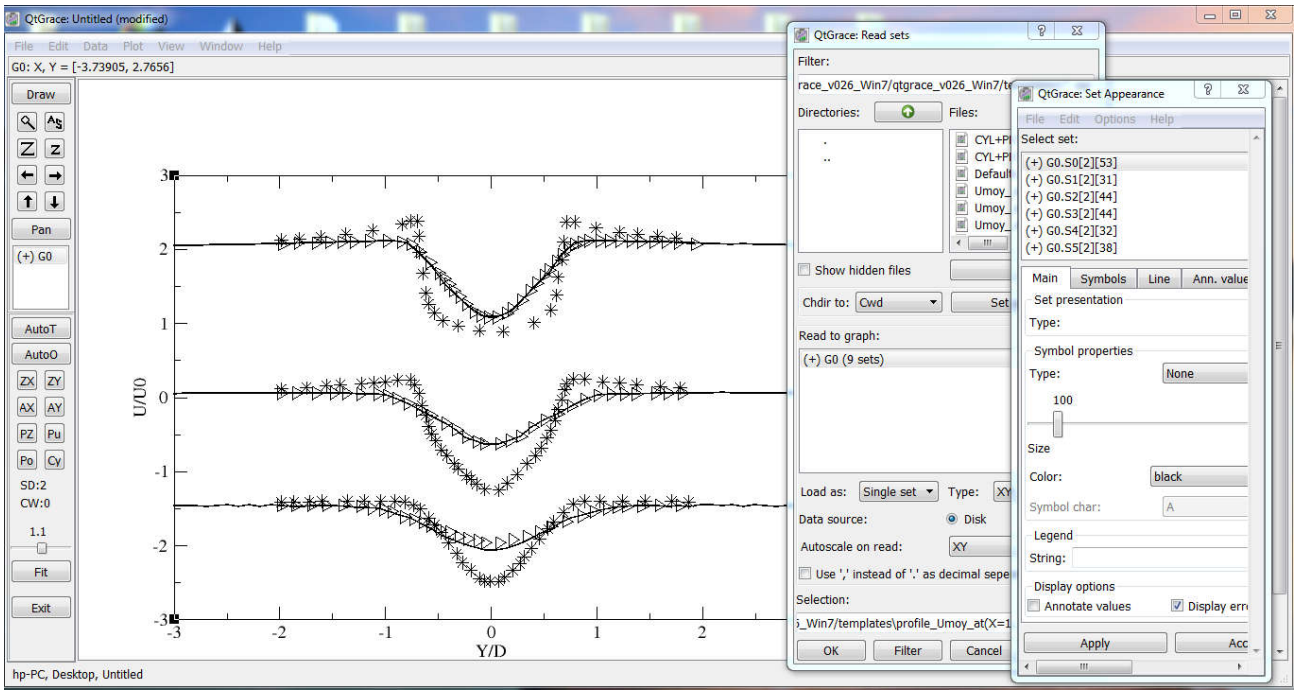

Fig.3.6: Preview of QtGrace, showing the Fourier transforms dialogue

Note:

All the software used in these simulations are**''FREE'' and some of them are ''OPEN SOURCE''**

CHAPTRE 4: STUDY CASES

Introduction:

Flow around a circular cylinder was intensively studied in the past and that returns to its simple geometry as well as the logical structure of the vortices. The studies were led on the one hand by academic interest and on the other hand by practical interest (industrial).

In this chapter we are going to study flow around a single circular cylinder with shape modification, to investigate the reduction of the drag. We will study flow over a smooth cylinder, grooved cylinder and a cylinder with a splitter plate. And for our simulations we will use Code_Saturne calculations software.

4.1.First case: Smooth Cylinder

Flow around a smooth cylinder is considered to be a prominent research topic in computational fluid dynamics (CFD). Although the geometry and mesh production are fairly simple,as shown in figure 01 below, the very complex nature of this flow makes calculations extremely difficult.

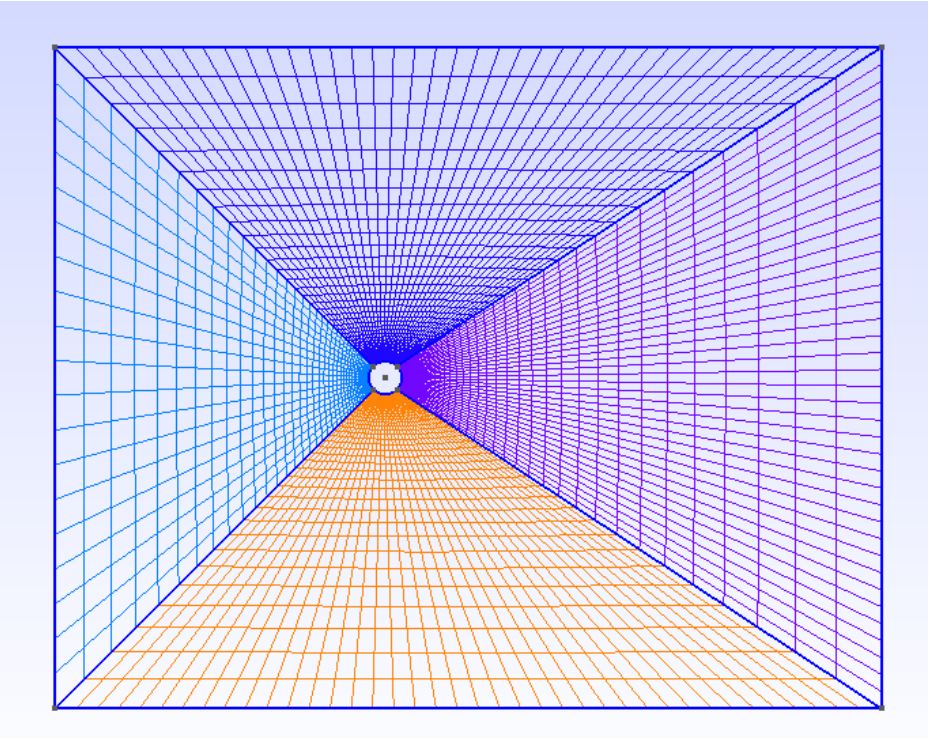

Fig.4.1: Structured mesh in the XY plane of smooth cylinder with Gmsh

4.1.1. Geometry

The geometry consists of an infinite cylinder mounted horizontally. The downstream length is set at 15 of diameter and the upstream length is set at 10 of diameter. The complete geometry is shown in Figure 4.2 Thegeometry and the boundary conditions remain the same for all tested cylinders.

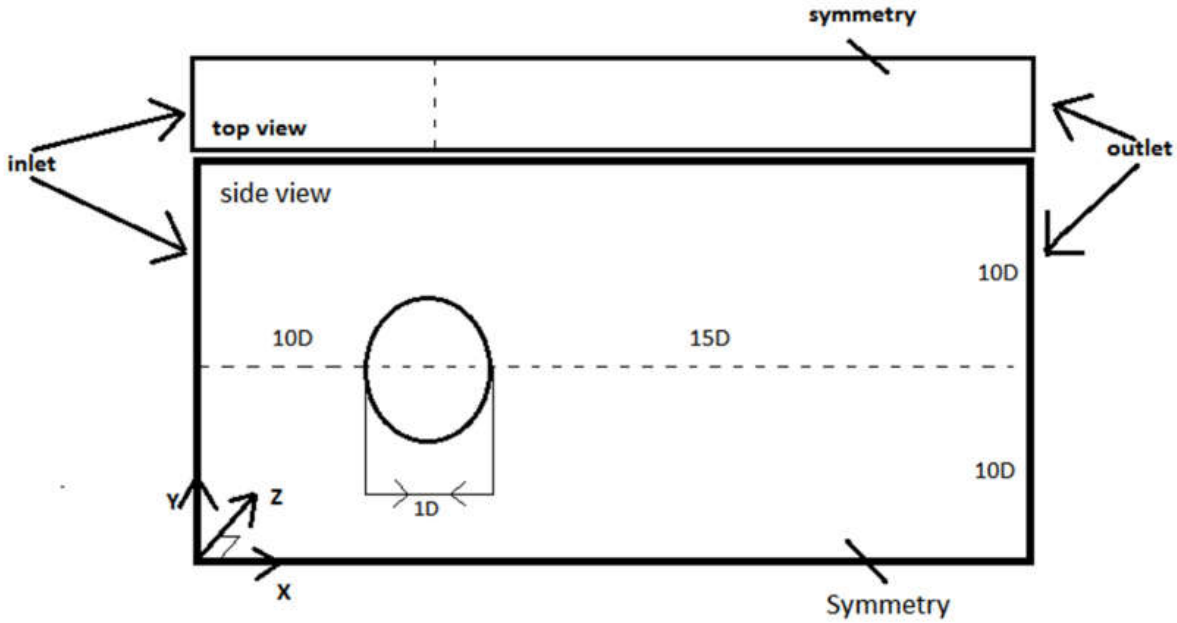

Fig.4.2: Geometry under consideration of infinite cylinder [16]

4.1.2. Physical parameters

The Reynolds number is based on the flow speed of the inlet (uniform speed without artificial and imposed turbulence) and the diameter of the cylinder we take: = 1 $andRe$ = 3900

4.1.3. Sensitivity study

A mesh sensitivity test with a comparison of four grids (magnified, medium, refined and over refined) was carried out, to define the best mesh to use for the next calculations.

	Nx	***Ny***	***Nz***	***N cells***
Coarse(a)	78	39	1	5304
Medium(b)	158	79	1	21804
Fine(c)	238	119	1	49504
Very Fine(d)	396	99	1	55044

Table 4.1Statistics of the grids of the smooth cylinder

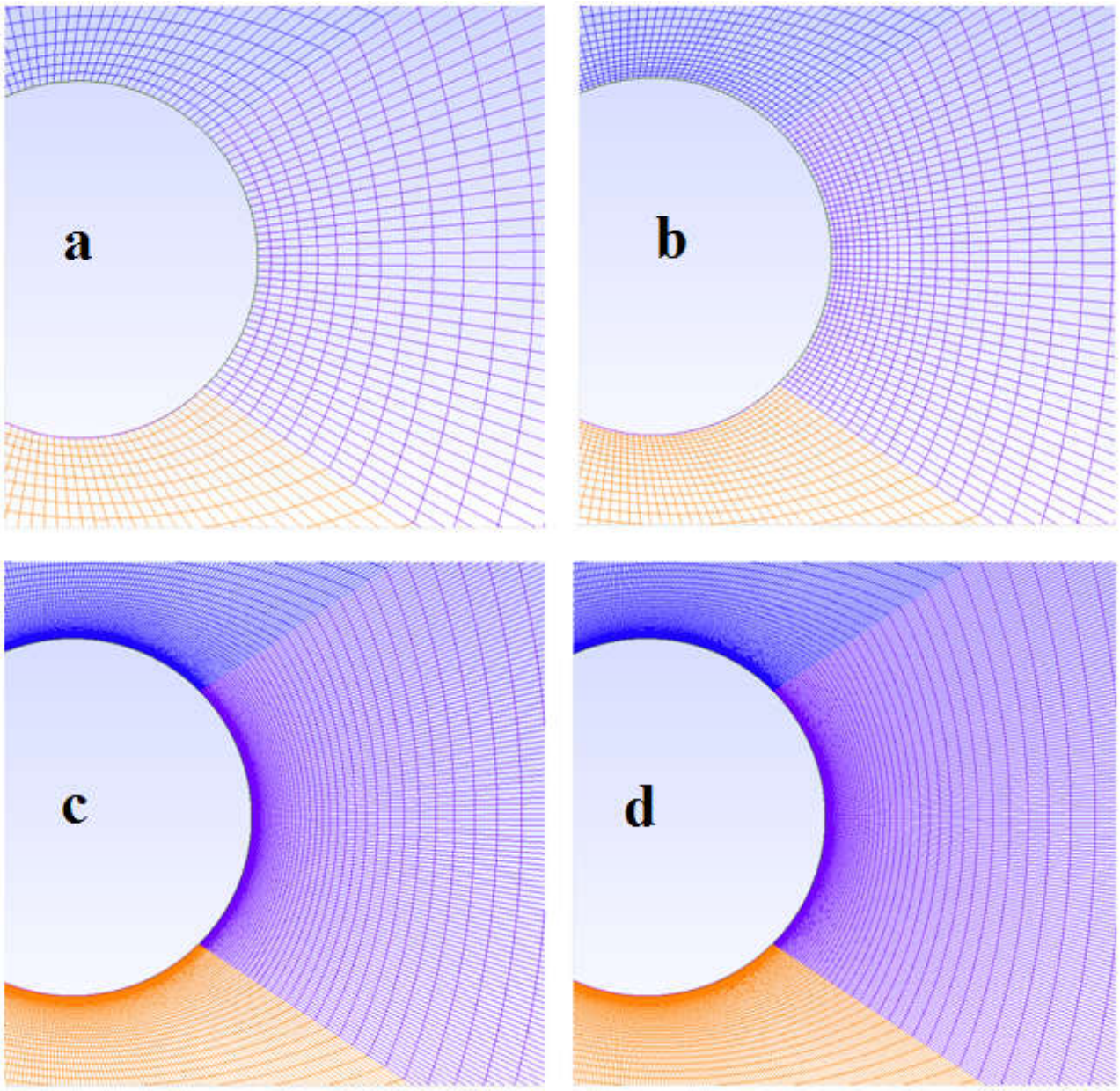

Fig.4.3: Zoom of the coarse(a), medium(b), fine(c) and very fine(d) mesh in the XY plane for the configuration of a smooth cylinder.

4.2.Second case: Grooved Cylinder

We kept the same shape of the first case with adding two longitudinal grooves on the external surface at 90° and 270° degrees, as shown in figure 4.4. The purpose of the present study is to investigate numericaly the drag reduction.

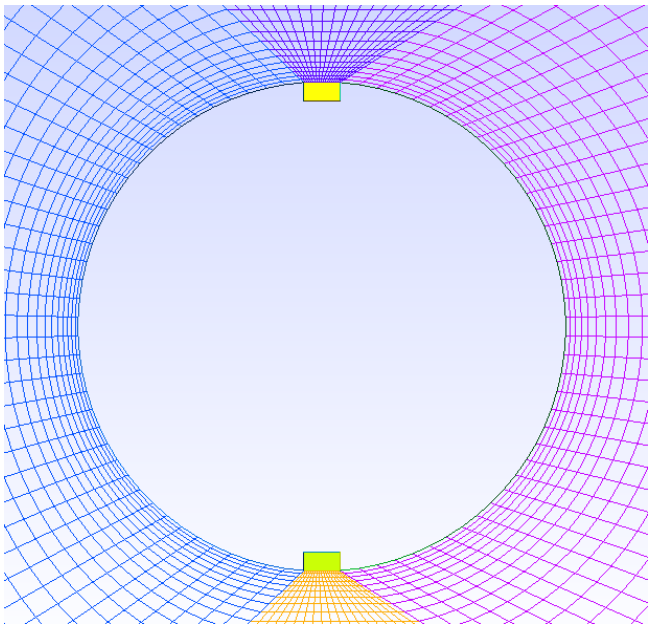

Fig.4.4: Zoom of the structured mesh of grooved cylinder

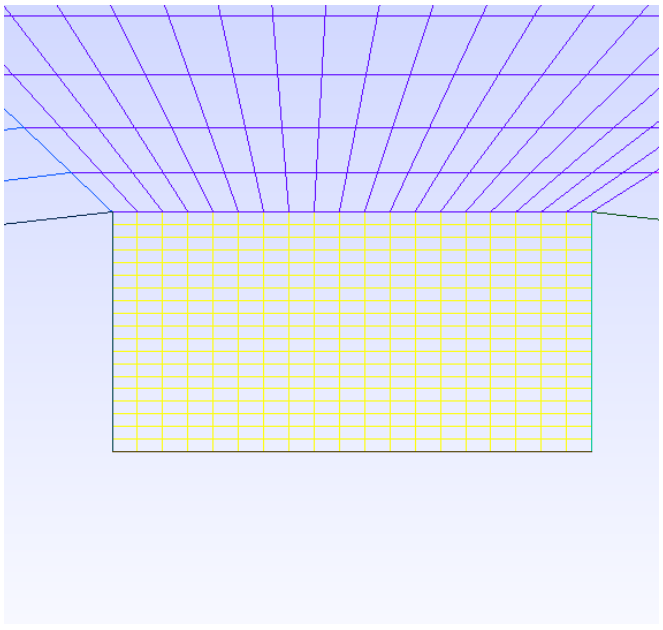

Fig.4.5: Zoom of the structured mesh of groove

4.2.1. Geometry

The geometry and the boundary conditions remain the same for all tested cylinders. As for the form and dimensions of the grooves, they are shown in Figure 4.5

S indicates the width of the groove,***h*** is the depth of the groove and***L*** is the length of the groove.

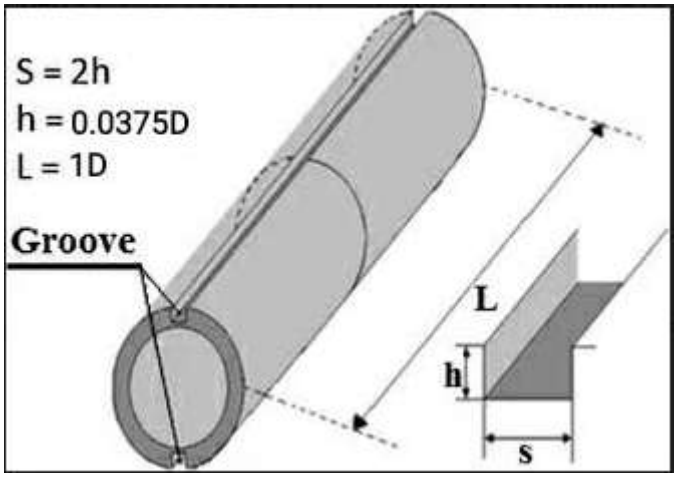

Fig.4.6: Form and dimensions of the grooves [41]

4.2.2. Physical parameters:

We will use a flow with Reynolds number$R_e = 9300$, and diameter of cylinder we take D=1 and we will use k - ω -sst) as a turbulence model.

4.2.3. Sensitivity study

	Nx	*Ny*	*Nz*	*N cells*
Coarse(a)	192	39	1	5246
Medium(b)	252	59	1	7966
Fine(c)	392	99	1	18546
Very Fine(d)	492	119	1	25016

Table 4.2 Statistics of the grids of the grooved cylinder

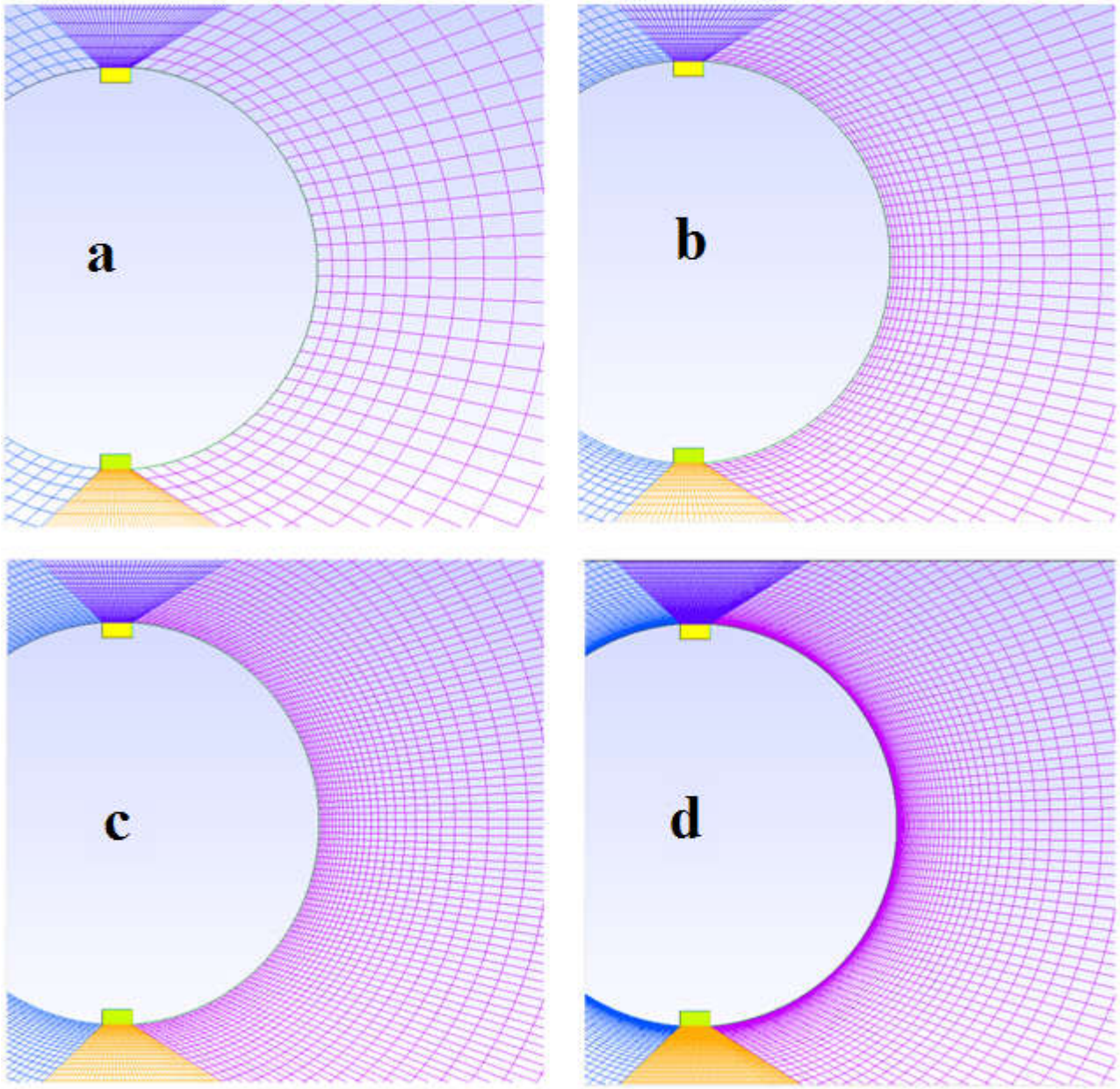

Fig4.7: Zoom of the coarse(a), medium(b), fine(c) and very fine(d) mesh in the XY plane for the configuration of a grooved cylinder.

4.3. Third case: Cylinder with flat plate

in this case we are going to inserting a splitter plate into the flow field(in the downstream, behind the wake),there are two main control parameters, which are the splitter plate length, L and the gap distance, G which is the distance from the rear cylinder surface to the leading edge of the splitter plate. In our case we will cancel the gap distance and take G=0, see the figure 4.5 below.

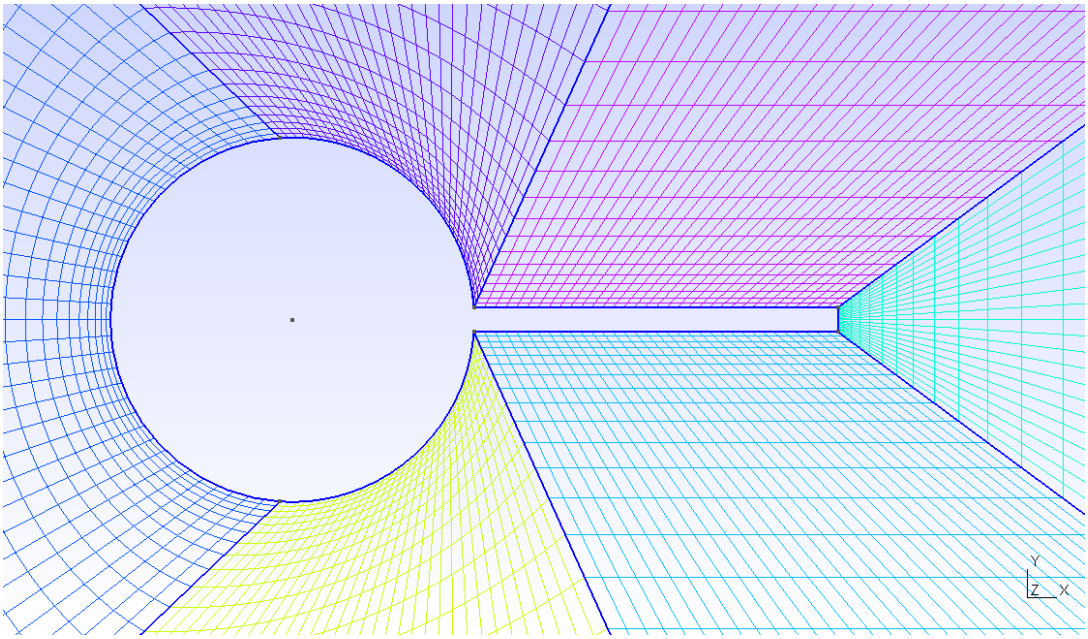

Fig.4.8: Zoom of the structured mesh in the XY plane of cylinder with a splitter plate with Gmsh

4.3.1. Geometry:

The geometry and the boundary conditions remain the same for all tested cylinders. The length of splitter plate is equal the cylinder diameter$L/D = 1$, with thickness $H = 0.067D$ and were attached to the rear of the circular cylinder (gap distance G=0). (All geometric parameters are consistent with the experimental of ***L.kai et al***) See figure 4.8bellow

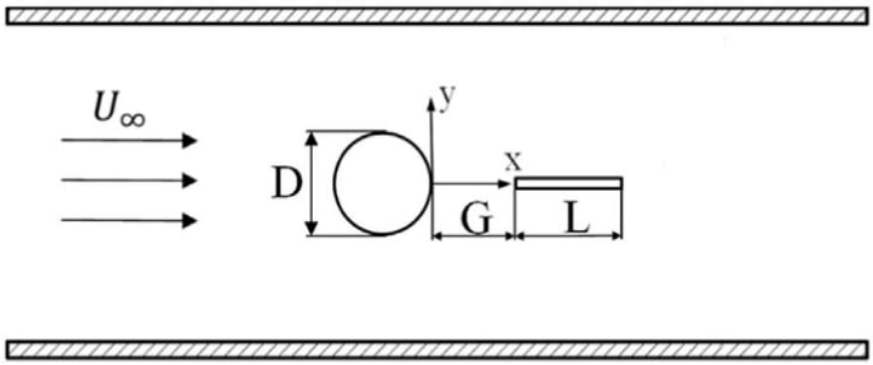

Fig.4.9: dimensions of splitter plate [13]

4.3.2. Physical parameters:

We will use a flow with Reynolds number$R_e = 3000$, and diameter of cylinder we take D=1 and we will use k - ω -sst) as a turbulence model.

4.3.3. Sensitivity study

	Nx	*Ny*	*Nz*	*N cells*
Coarse(a)	109	19	1	3161
Medium(b)	194	34	1	5626
Fine(c)	334	59	1	9686
Very Fine(d)	404	79	1	11716

Table 4.1Statistics of the grids of cylinder with plate

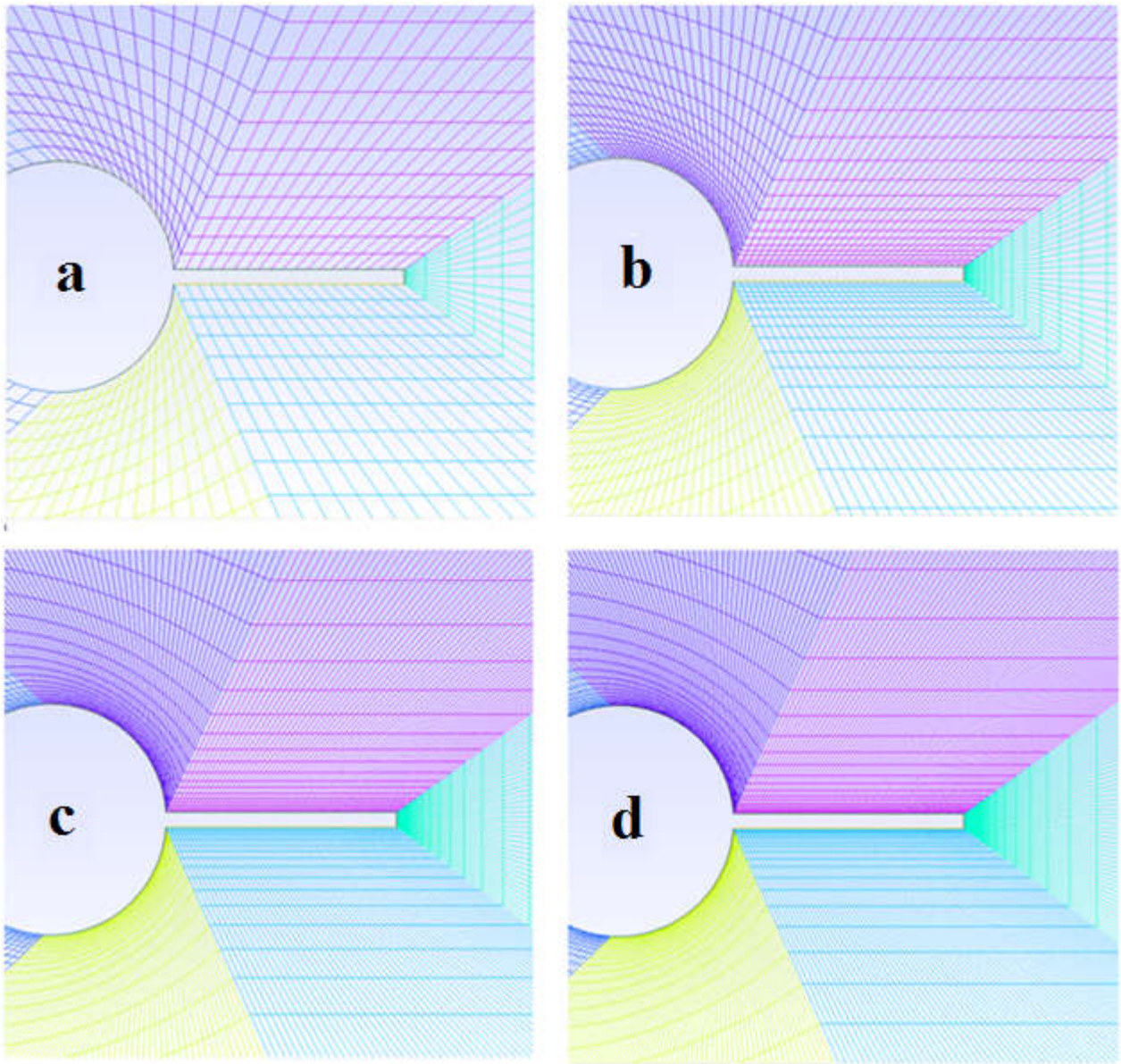

Fig.4.10:Zoom of the coarse(a), medium(b), fine(c) and very fine(d) mesh in the XY plane for the configuration of a cylinder.

CHAPTER 5: RESULTS AND DISCUSSION

Introduction

This chapter is dedicated to discussion and interpretation of the results of the performed numerical simulations. We will show the results of our cases, which are: flow around a single cylinder with a circular cross section and the modification of the geometric shape (smooth, slotted and plate cylinder). We use k - w - SST as turbulence model and then we will discuss the numerical results in comparison with the experimental results.

5.1. First Case: Smooth Cylinder

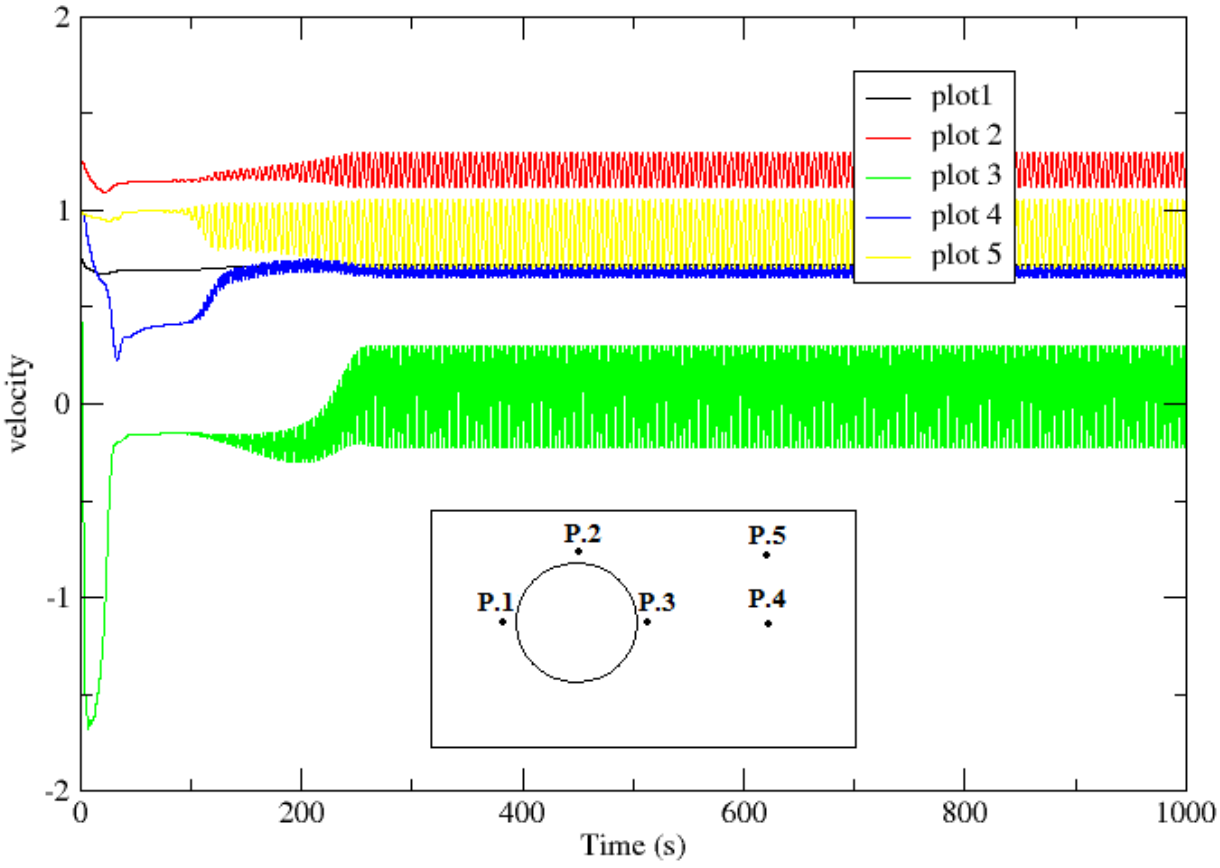

Fig.5.1. Calculations history for smooth cylinder (for each probe P)

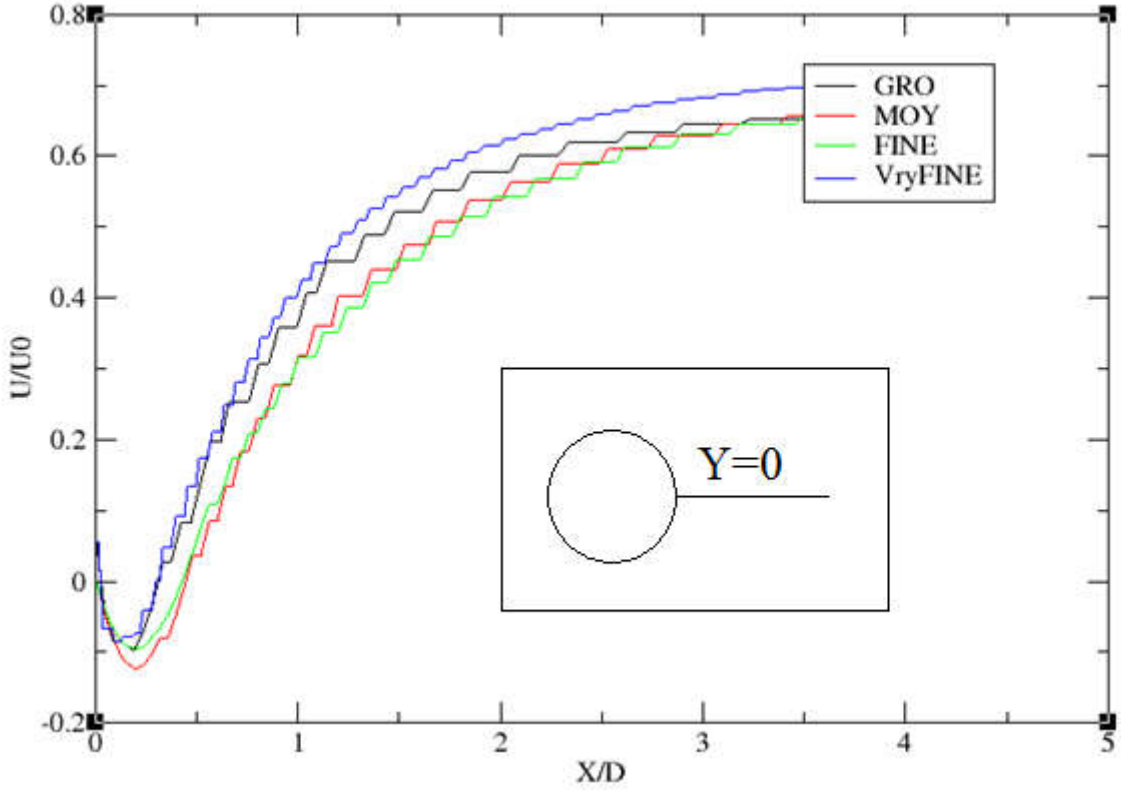

Fig. 5.2. Longitudinal mean velocity along the midline of the wake (Y / D = 0).

The longitudinal average velocity profiles along the wake axis (Y/D = 0) of the sensitivity study is shown in Figure 5.2. In this figure, when the mesh is more refined, the velocity profile has a slight deviation. Therefore, choose to use the fine grid for the following calculations

Study	Mode	Re
Z.RAHMANI et al [16]	RANS	3900
C.Norberg**[42]**	EXP	3000
P.Parnaudeau et al **[43]**	EXP	3900

Table.5.1: Previous studies used for comparison in the case of a single cylinder

5.1.1. Mean Velocity and Recirculation Length

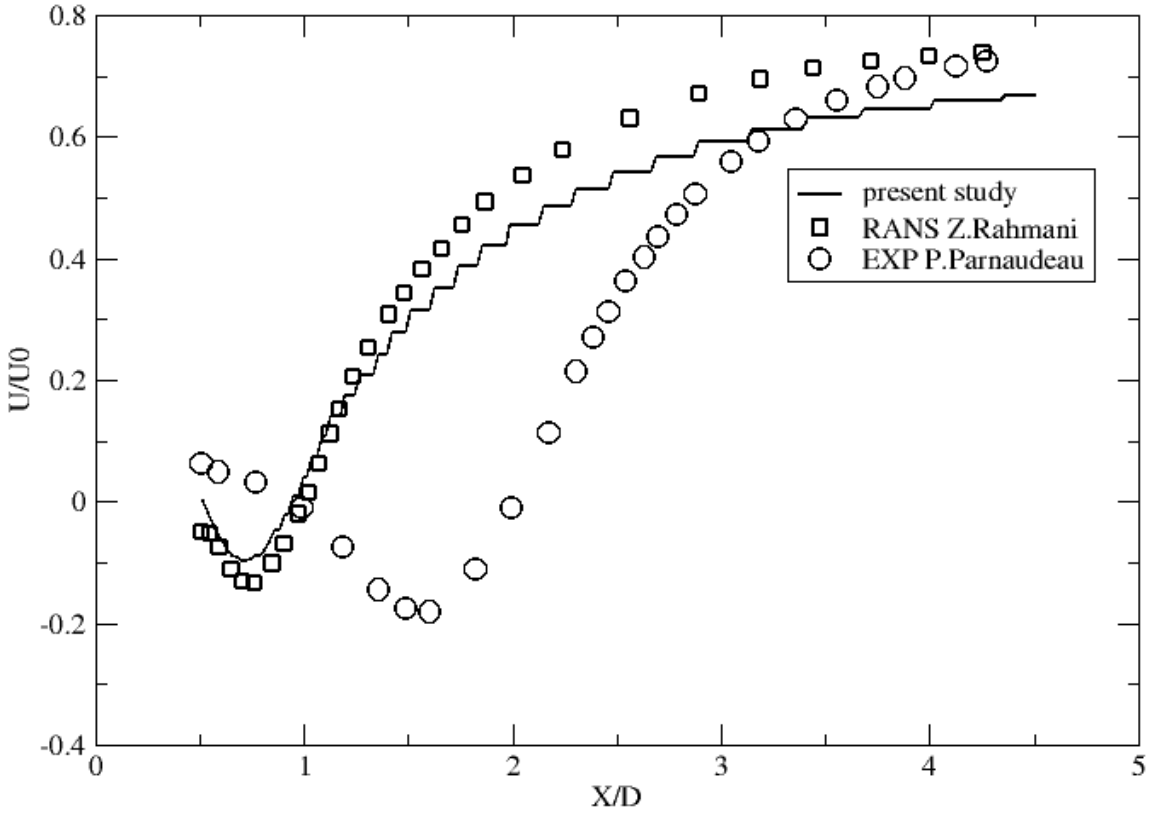

Fig.5.3. Longitudinal mean velocity along the midline of the wake (Y / D = 0). (−): present study, (□):RANS Z.Rahmani,(○)***:EXP P.Parnaudeau***

In order to compare the results of our RANS study with the results of numerical and experimental studies, we plotted the average velocity in the wake axis. From Figure 5.3, it can be seen that the Parnaudeau curve has the highest minimum velocity where $Umin = -0.22$. The difference that needs to be noted is that the loop length and maximum return speed in our RANS are less than other experimental values (parnaudeau). But we have the same speed curve with experimental and numerical results.

The longitudinal average velocity distribution in the wake region ($U/U0$) is shown in Figure 5.4 and analyzed at three points downstream of the cylinder ($X / D = 1.06, X / D = 1.54, X / D = 2.02$) . The transverse profile of the longitudinal velocity $U/U0$ shows that the velocity near the cylinder is insufficient. Due to the short recirculation length, a V-shaped profile is observed near the cylinder (at X / D = 1.06). This is consistent with the numerical data of Rahmani et al***[16]***, except for Parnaudeau***[43]*** et al, a U-shaped profile, as it moves away from the cylinder; the profile then evolves into a V-shape.

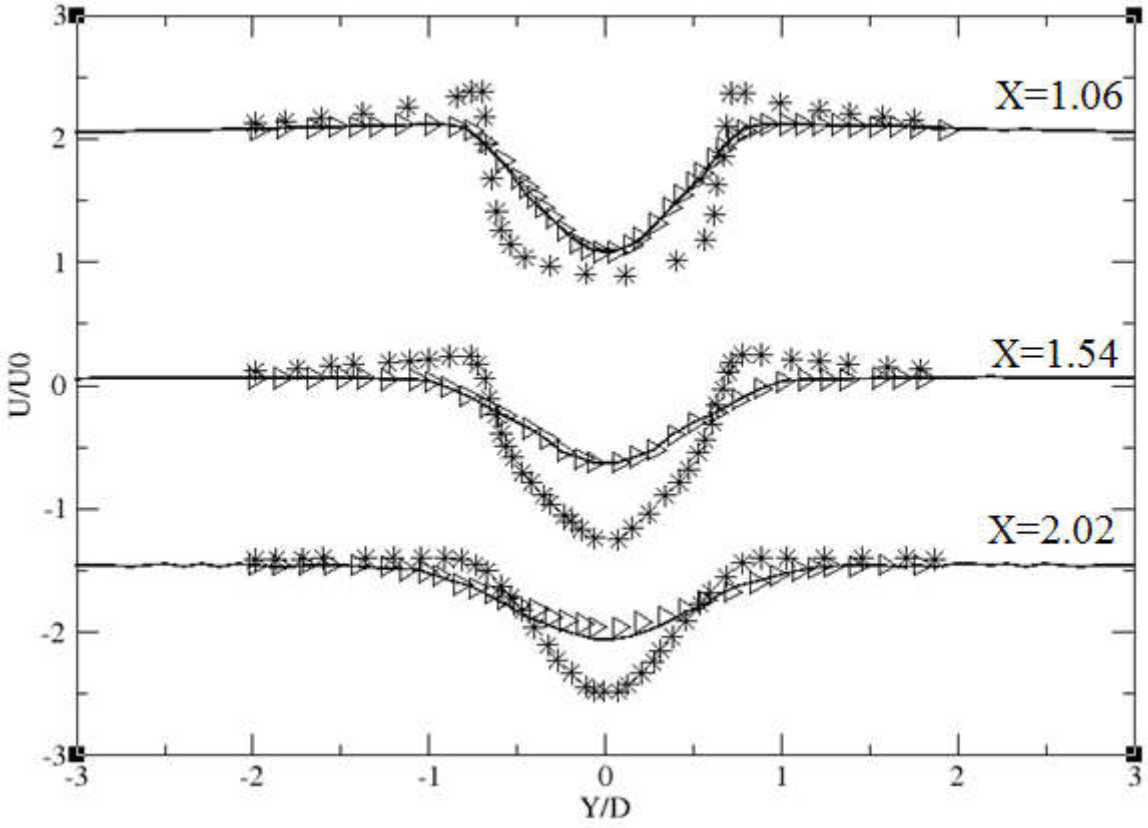

Fig.5.4. Mean stream wise velocity $(U/U0)$*at various* X/D*down-stream location at* $R_{D,u0} = 3900$, $(-)$*: Present study, (Δ): RANS Z.Rahman et al, (*): EXP Parnaudeau et al*

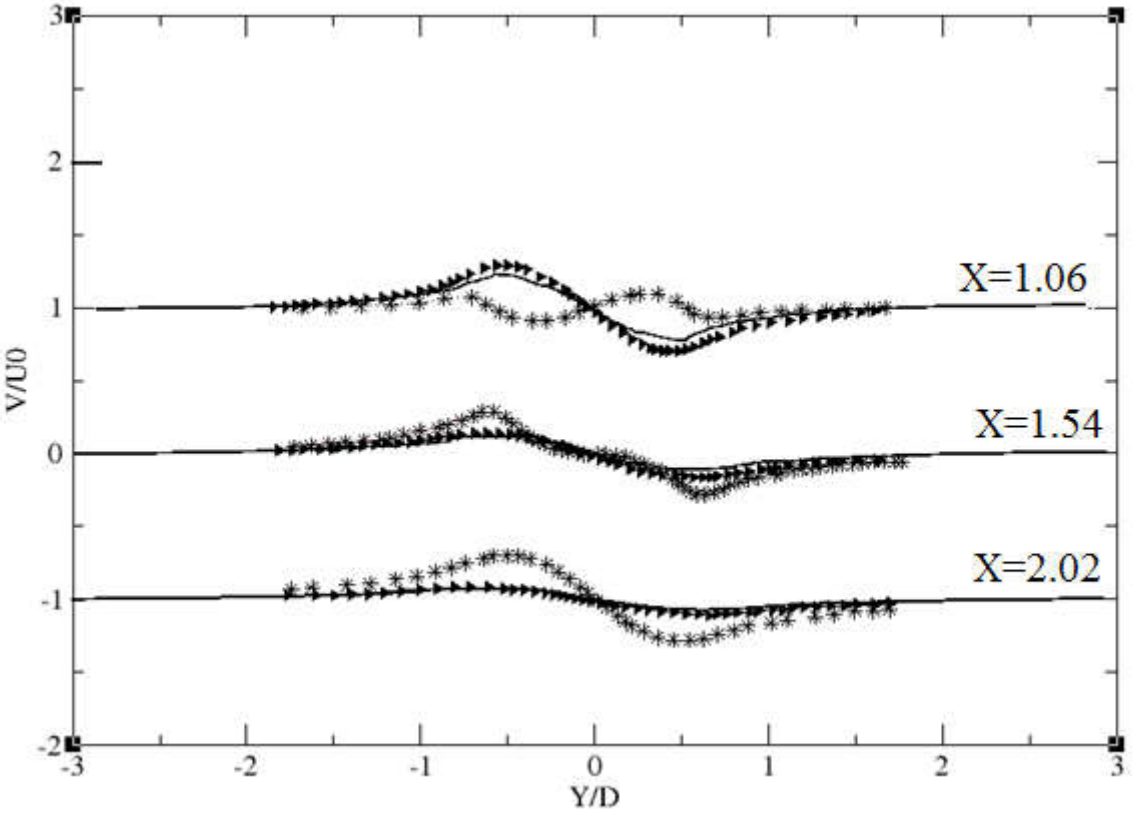

Fig.5.5. Mean cross-stream velocity $(V/U0)$*at various* (X/D) *down-stream locations at*$R_{D,u0} = 3900$. $(-)$*: Present study, (Δ): RANS Rahmani et al, (*): EXP Parnaudeau et al*

Figure 5.5 shows the cross flow ($V/U0$)velocity profile. In the wake of a single cylinder, it is located at $R_e = 3900$. In this figure, the velocity ($at\ X/D = 1.06$) is directed beyond the symmetry line($Y/D = 0$). This tendency is reversed as we approach the symmetry line at points X / D = 1.54 and X / D = 2.02. The comparison of our RANS results is consistent with the measurements of Zakaria Rahmani et al ($with\ X/D = 1.06$) and with the measurements of Parnaudeau et al[43]. ($with\ X/D = 1.54$). The profile in position X / D = 2.02 still differs from other data.

5.1.2. Mean Pressure Coefficient

The distribution of the mean pressure coefficient ($\overline{C_P}$) around the cylinder is plotted in Figure5.7; we use the mathematical relation below to calculate the average pressure coefficient

$$\overline{C_P} = {2(\bar{P} - P_\infty)}\Big/{(\rho_\infty u_\infty^2)} \qquad (5.1)$$

It is compared to the experimental results of RANS Rahmani et al [16] for a Reynolds number equal to 3900.

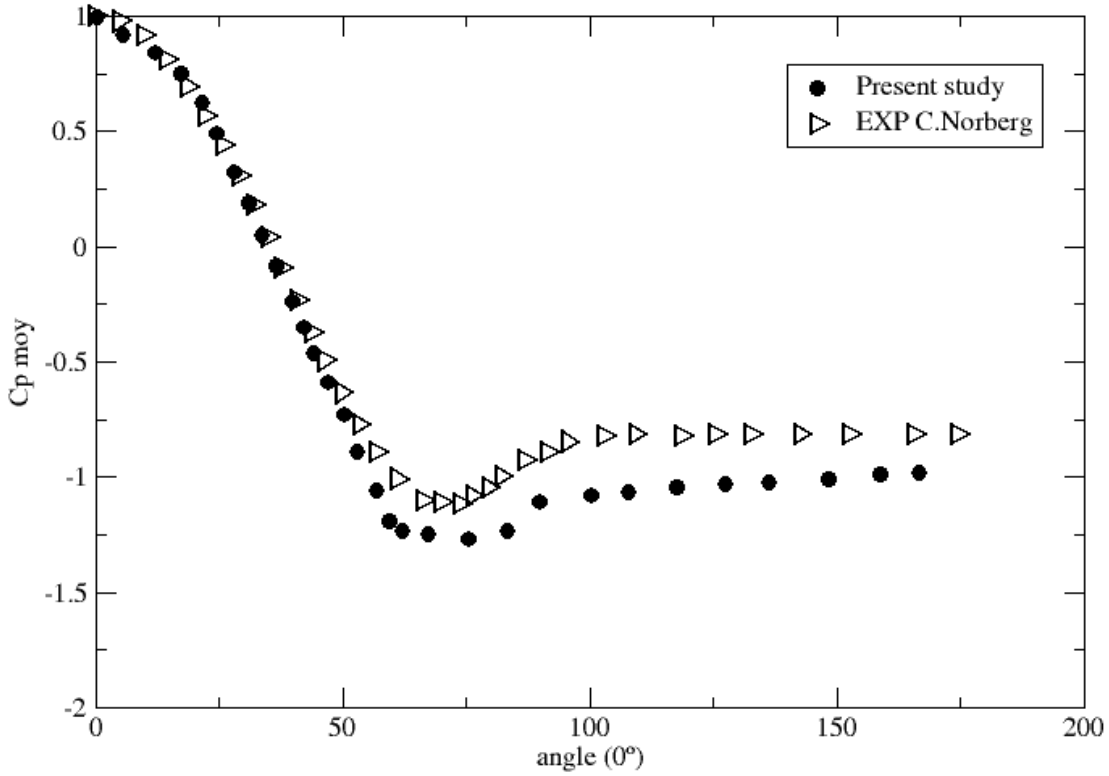

Fig.5.6.Mean pressure coefficient profile around a single cylinder.
(●): Present study($R_e = 3900$),(Δ):C.Norberg($R_e = 3000$)

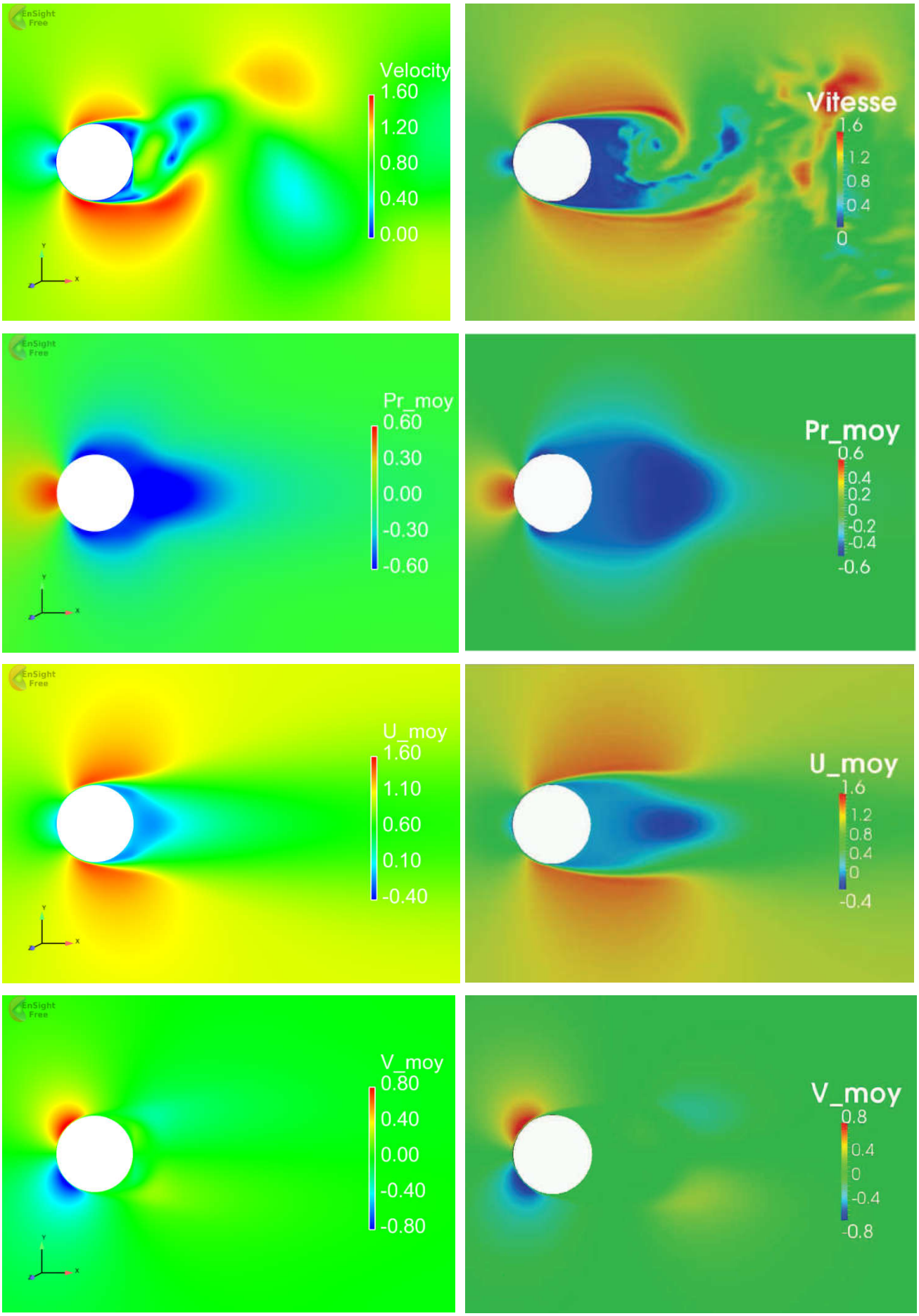

Fig.5.7.Comparison of the different fields of the flow.

(Left) Present study, (right) LES Afgan et al

Figure.5.6. shows the distribution of$\overline{C_P}$ around the surface of a smooth cylinder. The $\overline{C_P}$ reaches maximum values at the leading edge $\overline{C_P}max = 1$ for an angle$\theta = 0°$, it decreases to a minimum value $\overline{C_P}min = -1.28$ for an angle $\theta = 80°$. In the wake, there are a little disparities between the numerical and experimental results where start at angle $\theta = 50°$. However we have the same $\overline{C_P}$ curve,inspite we used RANS simulation but our results were close to experimetal ones. It is noted that the distribution of $\overline{C_P}$is symmetrical with respect to the 180 ° angle.

In figure 5.7, the quantities of the flow were compared (mean velocity and pressure fields) of the results of the present study with the numerical results (LES) of Afgan et al.

5.2. The Second Case: Grooved Cylinder

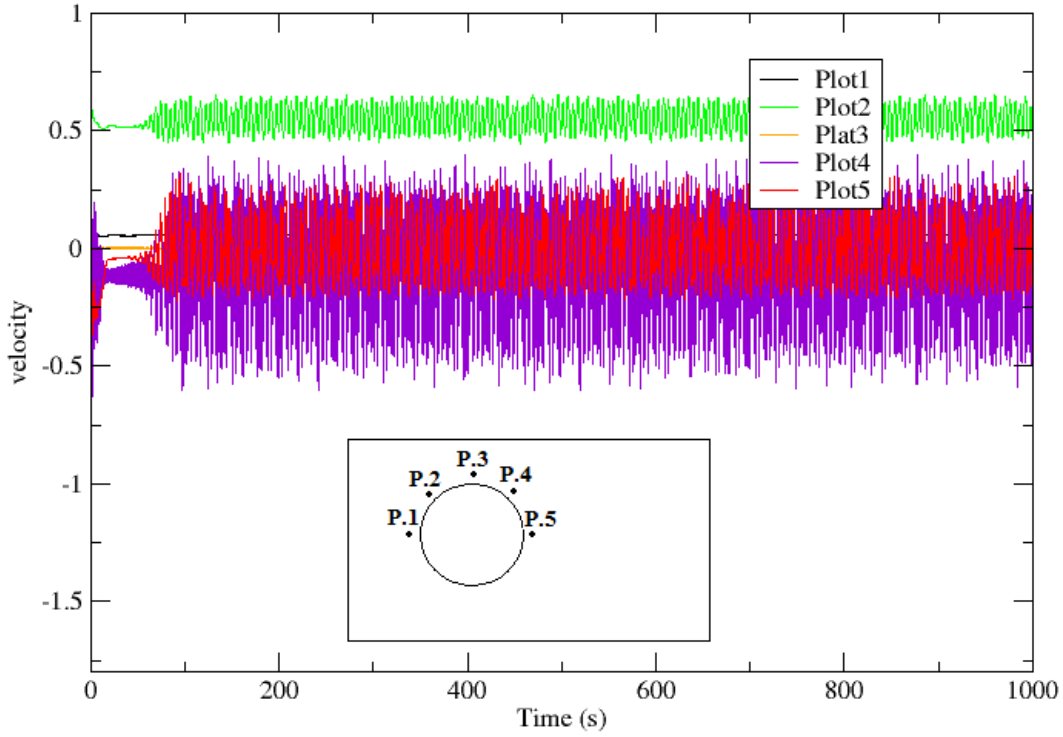

Fig.5.8. Calculations history for grooved cylinder

The longitudinal mean velocity profiles along the wake axis (at $Y / D = 0$) for this sensitivity study are shown in Figure5.9. In this figure there is a little deviation in the velocity profile, when the mesh is more refined. Thus, the choice was made to take the fine mesh for the following calculations

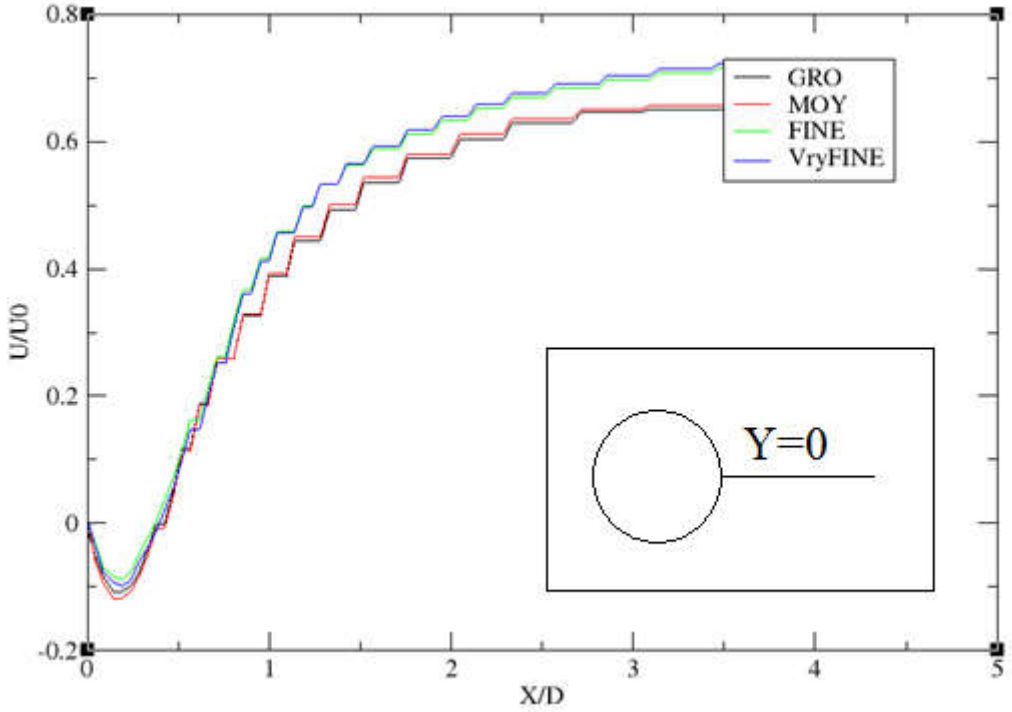

Fig.5.9. Sensitivity study for the longitudinal mean velocity along the midline of the wake (Y / D = 0).

The table.5.2 shows some experimental and numerical studies that performed on grooved cylinder, in order to compare these results with our RANS study results

Study	Mode	Re
O. Ladjedel et al**[7]**	RANS / Exp	$Re = 20000$
O. Ladjedel et al**[11]**	Exp	$Re = 2 * 10^4, 5 * 10^4, 7 * 10^4$
T. Yahiaoui**[41]**	Exp	$Re = 9300$

Table.5.2: Previous studies used for comparison in the case of a single cylinder

5.2.1. Mean Velocity and Recirculation Length

In order to compare the results of our RANS study for a grooved cylinder with the results the First case (Smooth cylinder), we plotted the average velocity in the wake axis. From Figure 5.10,it can be seen that both cases has the same curve with a little deviation where start at X/D=1.5

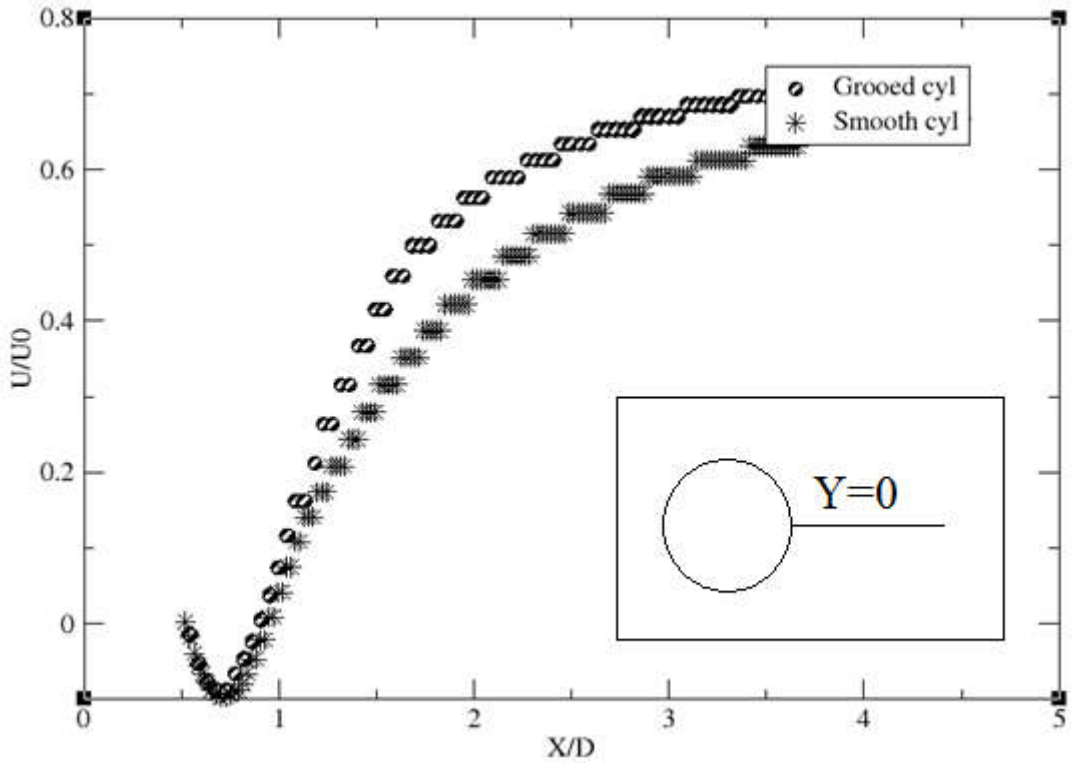

Fig.5.10. Mean stream-wise velocity along the wake centerline $(Y/D = 0)$*for a single cylinder: (●): Grooved cylinder at* $R_e = 9300$*; (*): Smooyh cylinder at* $R_e = 3900$

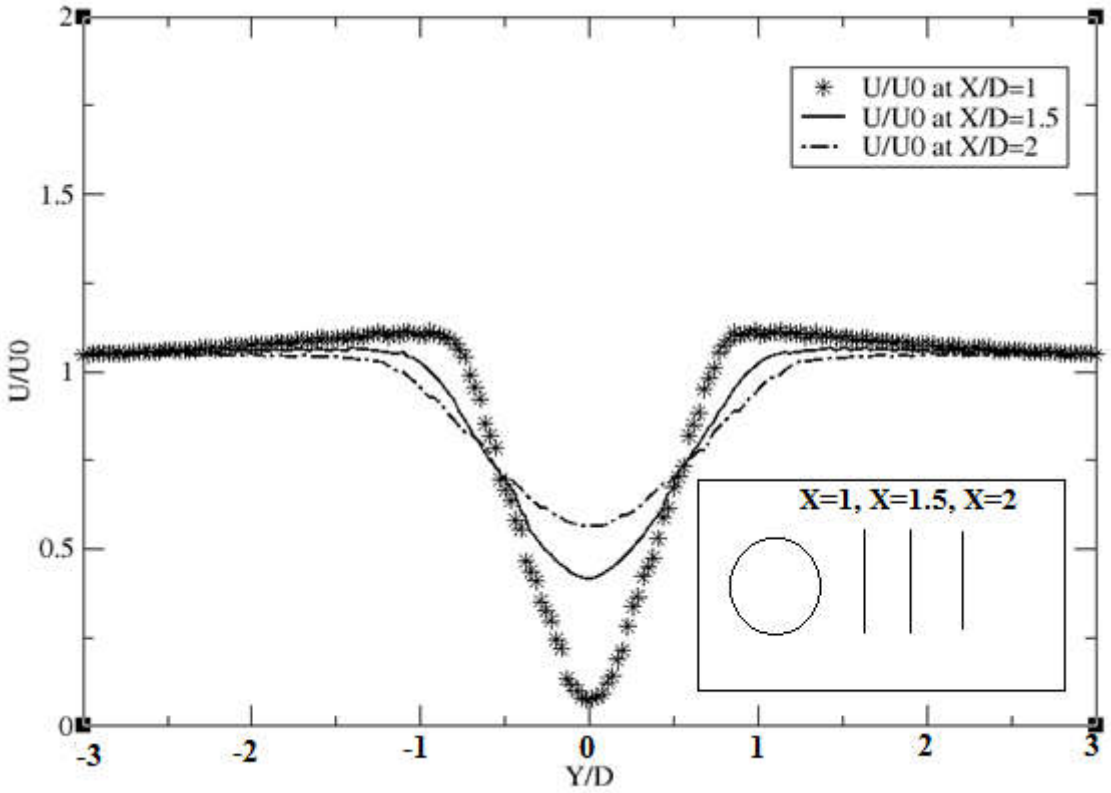

Fig.5.11. Mean stream wise velocity $(U / U0)$*at various* X/D *down-stream location at* $Re = 9300$

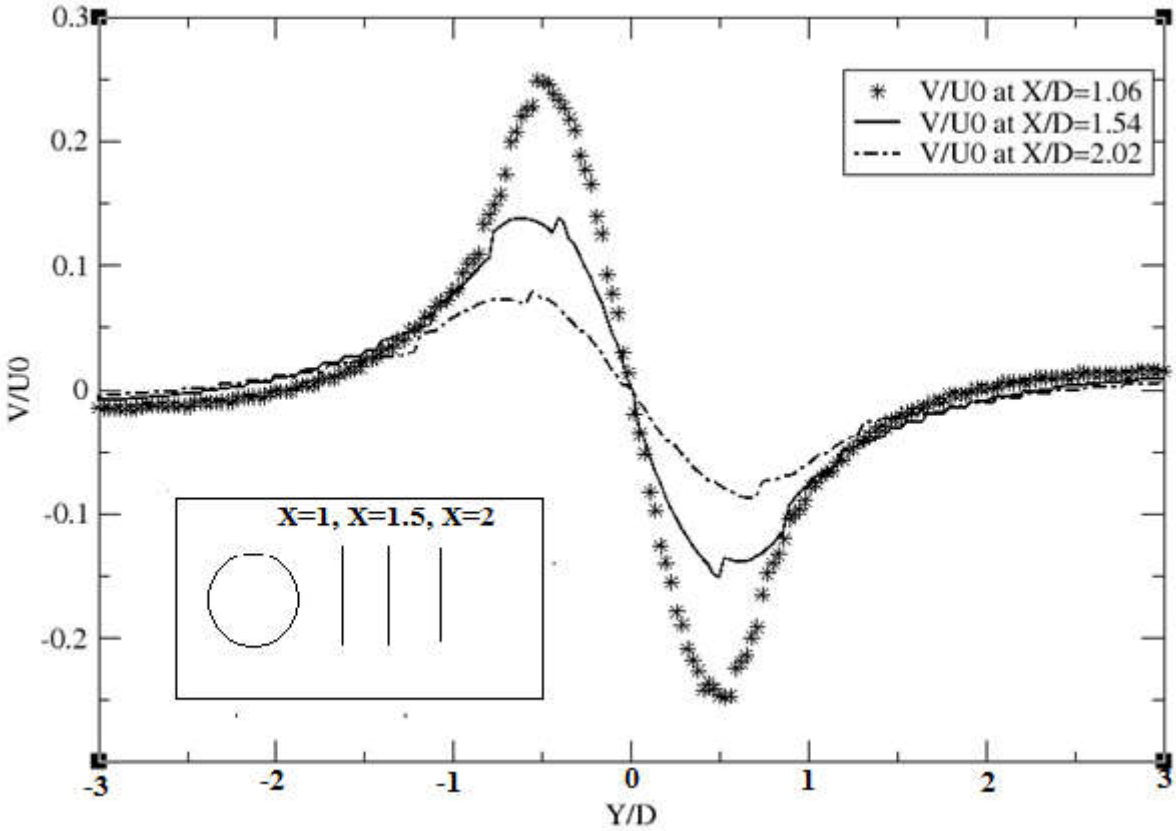

Fig.5.12. Mean cross-stream velocity $(V / U0)$ ***at various*** X/D ***down-stream locations at*** $Re = 9300$.

In the figures5.11 and 5.12 we present the mean stream-wise $(U/U0)$ and crosse-stream $(V/U0)$velocity profiles respectively, in the wake of the single cylinder at $Re = 9300$, the results were taken at three points $(X/D = 1{,}06,\ X/D = 1{,}54,\ X/D = 2{,}02)$ behind the cylinder.

5.2.2. Mean Pressure Coefficient

The distribution of the mean pressure coefficient $(\overline{C_P})$around the cylinder is plotted in Figure5.10; It is compared to the experimental results ofTayab YAHIAOUI et al [44] for a Reynolds number equal to 9300.

Figure.5.13 presentthe distribution of $\overline{C_P}$ around the surface of the grooved cylinder. The $(\overline{C_P})$ reaches maximum values at the leading edge $\overline{C_P}max = 1$ for an angle $\theta = 0°$, it decreases to a minimum value $\overline{C_P}min = -1.9$ for an angle $\theta = 86° - 94°$ (which is groove location). Consequently, there are disparities between the numerical and experimental results. However, our RANS results were acceptable and realistic. It is observed that the distribution of $\overline{C_P}$ is symmetric with respect to the 180 ° angle.

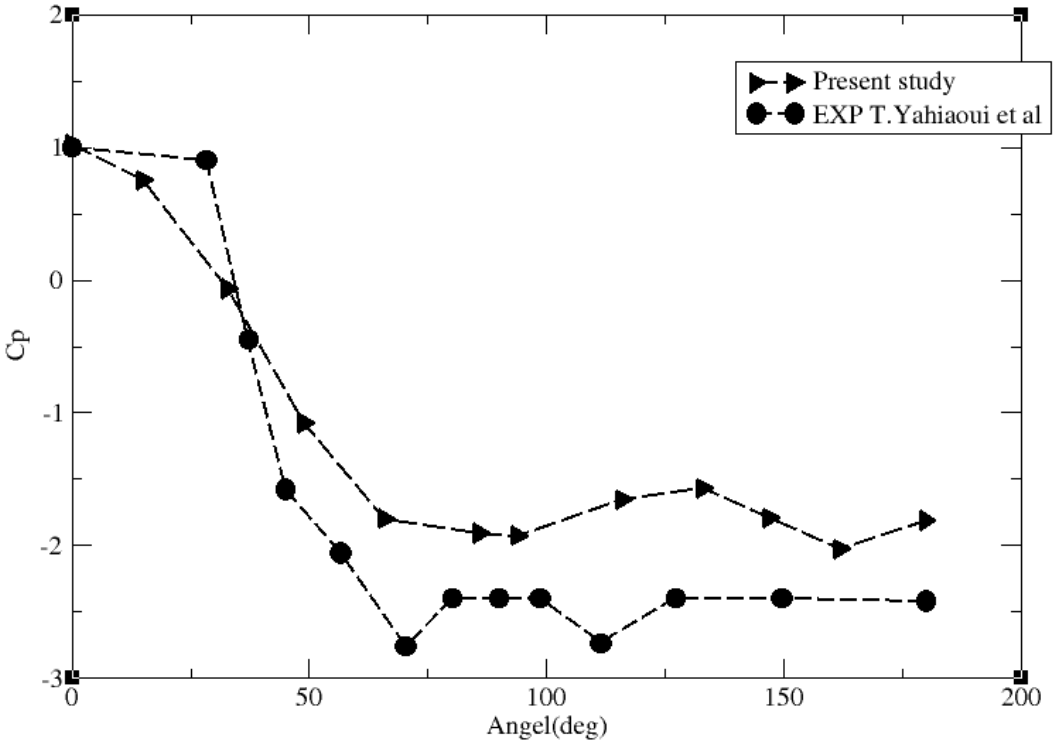

Fig.5.13. Mean pressure coefficient profile around a grooved cylinder.
(►): Present study($R_e = 9300$),(●): ExpT.Yahiaoui et al($R_e = 9300$)

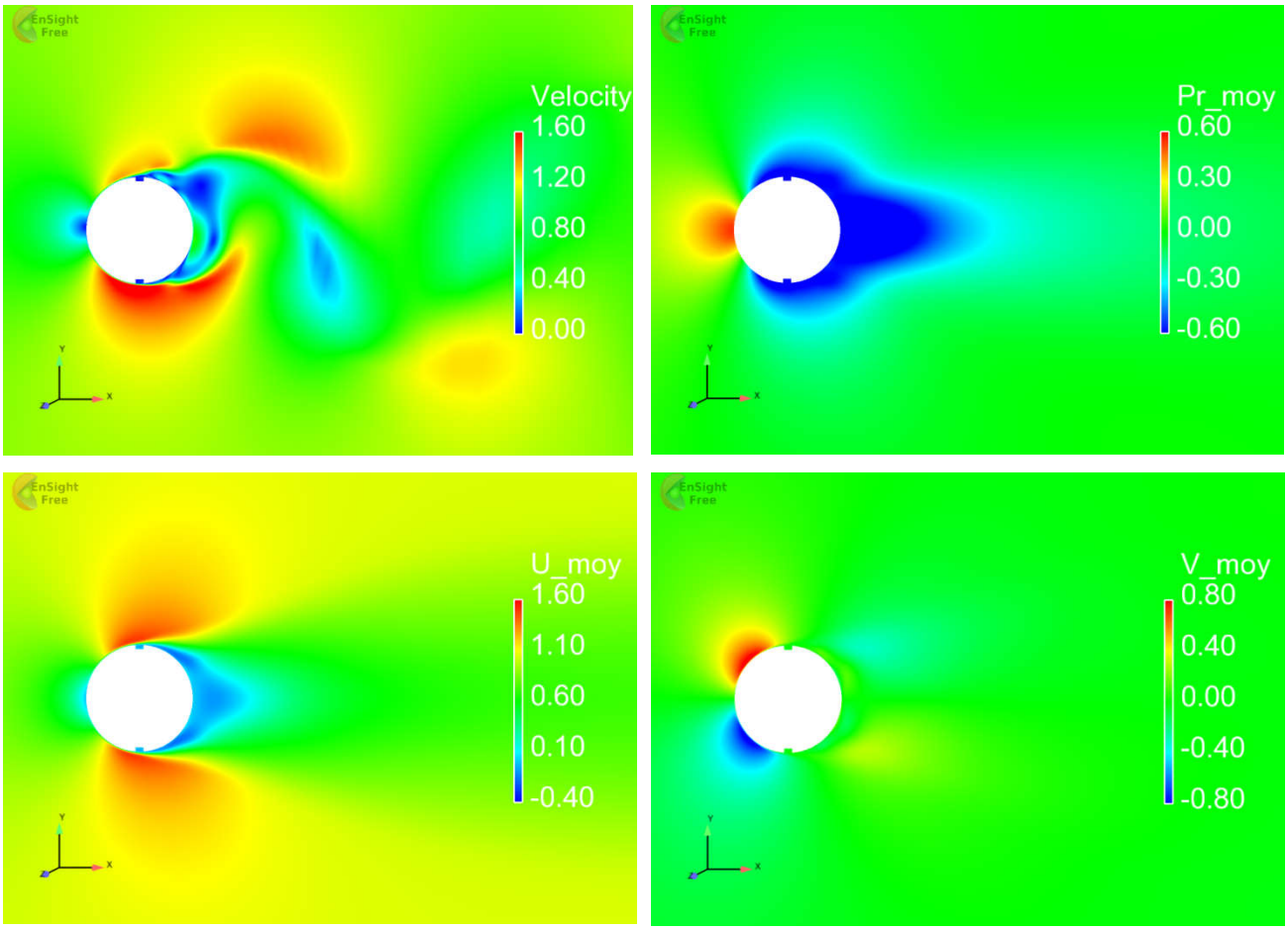

Fig. 5.14.Different fields of the flow

The figure 5.14 Shows the quantities of flow (mean velocity and pressure fields) of the present studyresults

5.3. The Third Case: Cylinder with Plate Flat

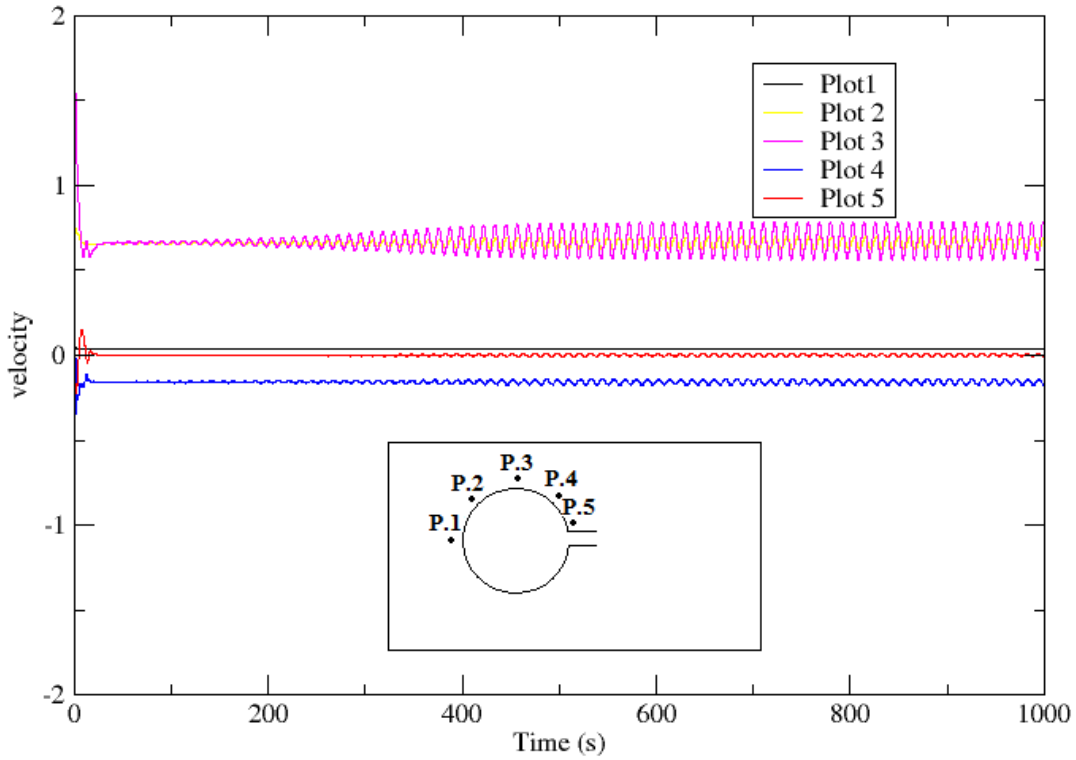

Fig.5.15. Calculations history for cylinder with plate

The figures 5.1, 5.8 and 5.15 present the calculation history of smooth cylinder, grooved cylinder and cylinder with flat plate respectively. Therefore capture the different quantities of our flow, we added five probes around the cylinder.

In order to investigate the convergence of our calculation, we plotted the velocity variations which captured by probes, with time, in each case. The results showed that all calculations are converged after 2500 iteration (250 time (s)), but it began at different time for each case. We notice that each probe has a different velocity values and that return to its location.

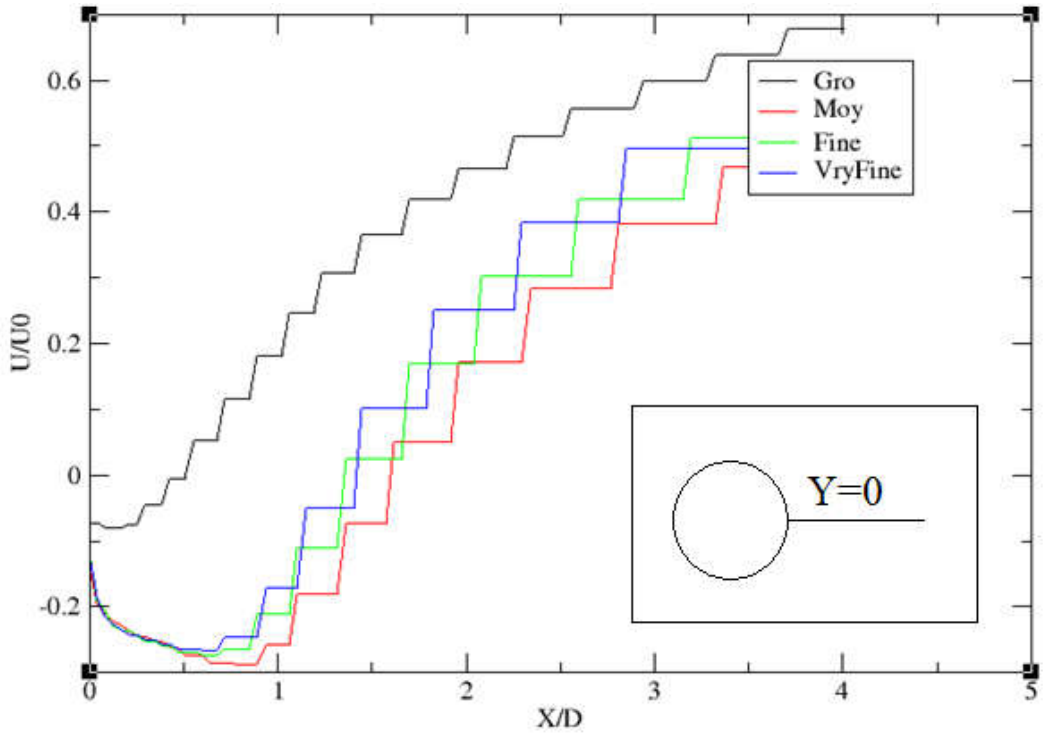

Fig.5.16. Sensitivity study for the longitudinal mean velocity along the midline of the wake (Y / D = 0).

The longitudinal mean velocity profiles along the wake axis (at $Y / D = 0$) for this sensitivity study are shown in Figure5.16. In this figure there is a little deviation in the velocity profile, when the mesh is more refined. Thus, the choice was made to take the fine mesh for the following calculations

5.3.1. Mean Velocity and Recirculation Length

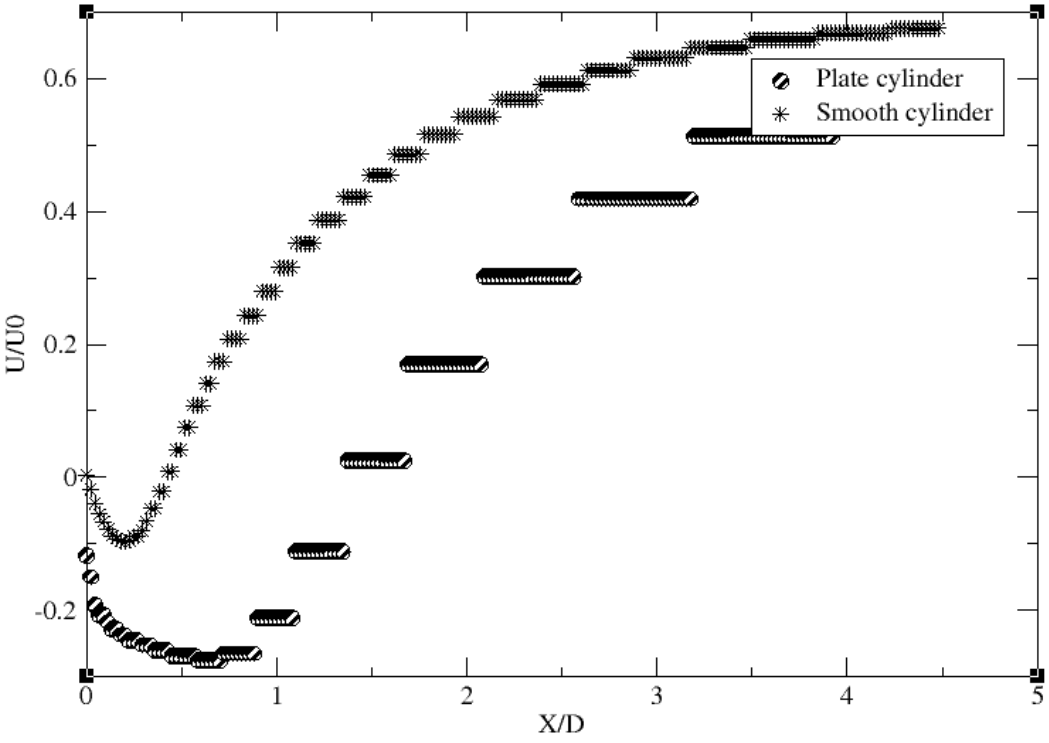

Fig.5.17: Mean stream-wise velocity along the wake centerline $(Y/D = 0)$ ***for a single cylinder: (●): Cylinder with plate at*** $R_e = 3000$***; (*): Smooyh cylinder at*** $R_e = 3900$

To compare the results of our RANS study for a plate cylinder with the results of the First case (smooth cylinder), we plot the average velocity on the wake axis. As shown in Fig.5.17

It can be seen that the plate cylinder curve has the highest minimum velocity where U/U0 reach$-0.25(D/D0_{min} = -0.25)$. The difference that needs to be noted is that the loop length and maximum return speed in case of cylinder with plate is less than other cylinder values. But we have the same speed curve in both results.

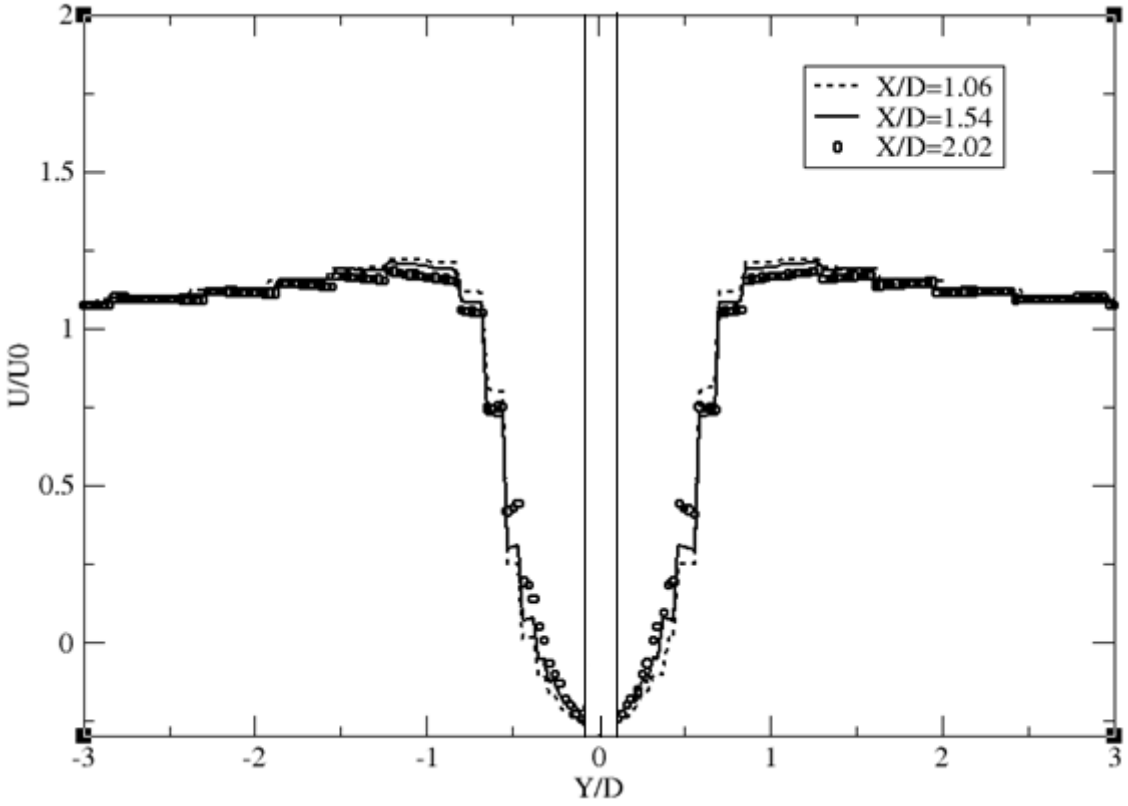

Fig.5.18: Mean stream wise velocity $(U / U0)$***at various*** X/D ***down-stream location at*** $R_e = 3000$

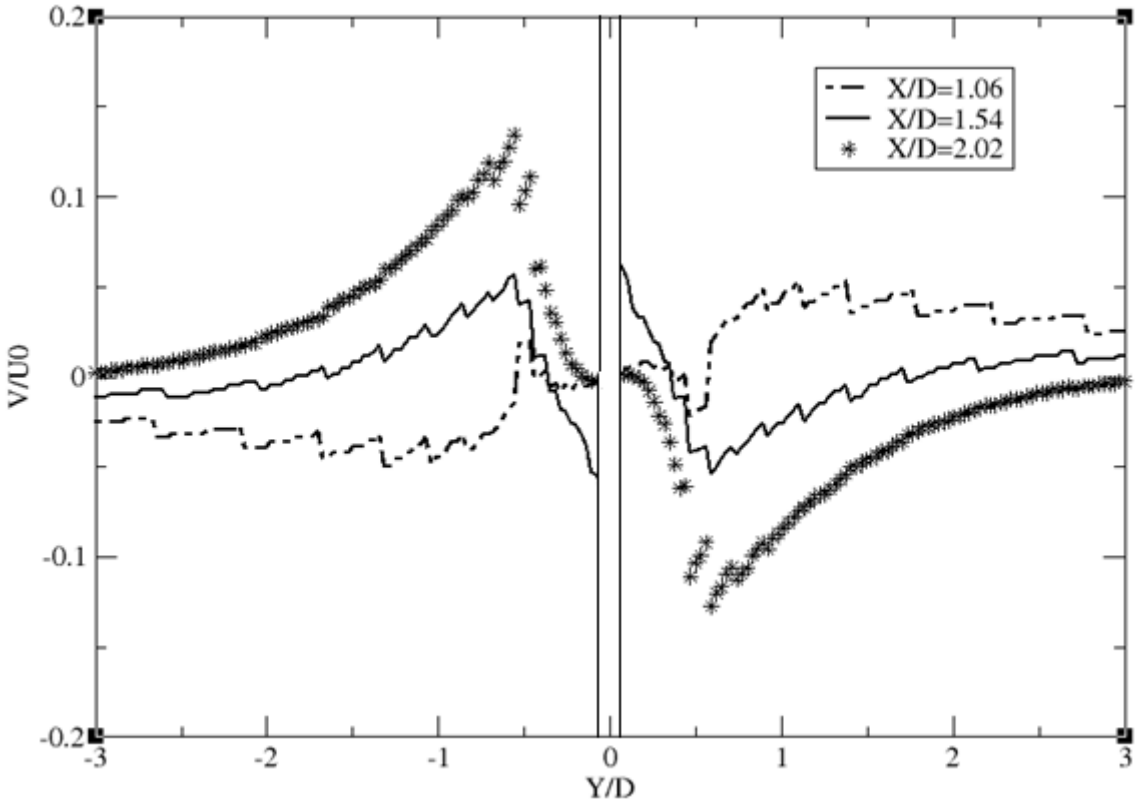

Fig.5.19: Mean cross-stream velocity $(V / U0)$ ***at various*** X/D ***down-stream locations at*** $R_e = 9300$.

5.3.2. Mean Pressure Coefficient

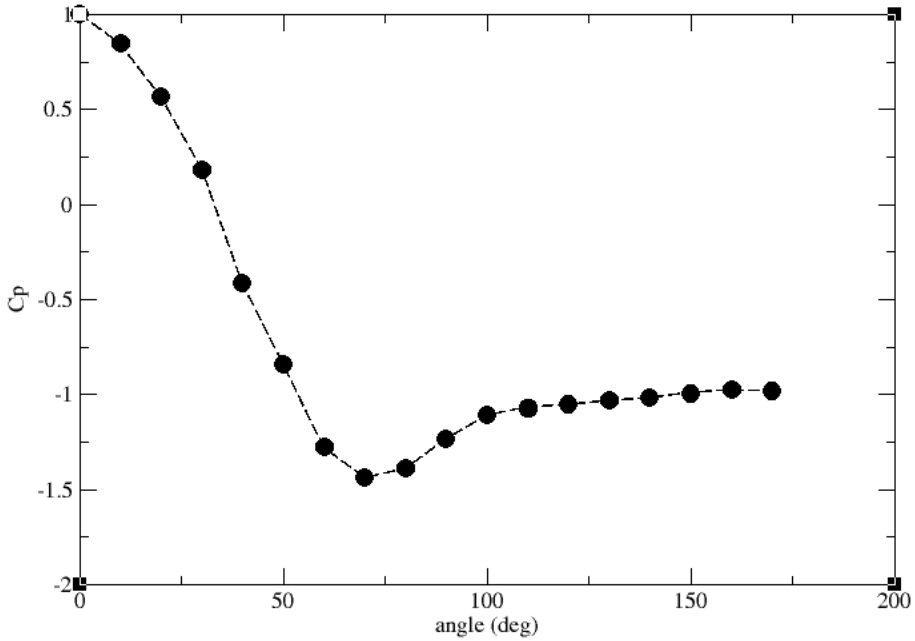

Fig.5.20. Mean pressure coefficient profile around a single cylinder with plate.

Figure.5.20. shows the distribution of $\overline{C_P}$ around the surface of the cylinder. The $\overline{C_P}$ reaches maximum values at the leading edge $\overline{C_P}max = 1$ for an angle$\theta = 0°$, it decreases to a minimum value $\overline{C_P}min = -1.44$ for an angle $\theta = 70°$.

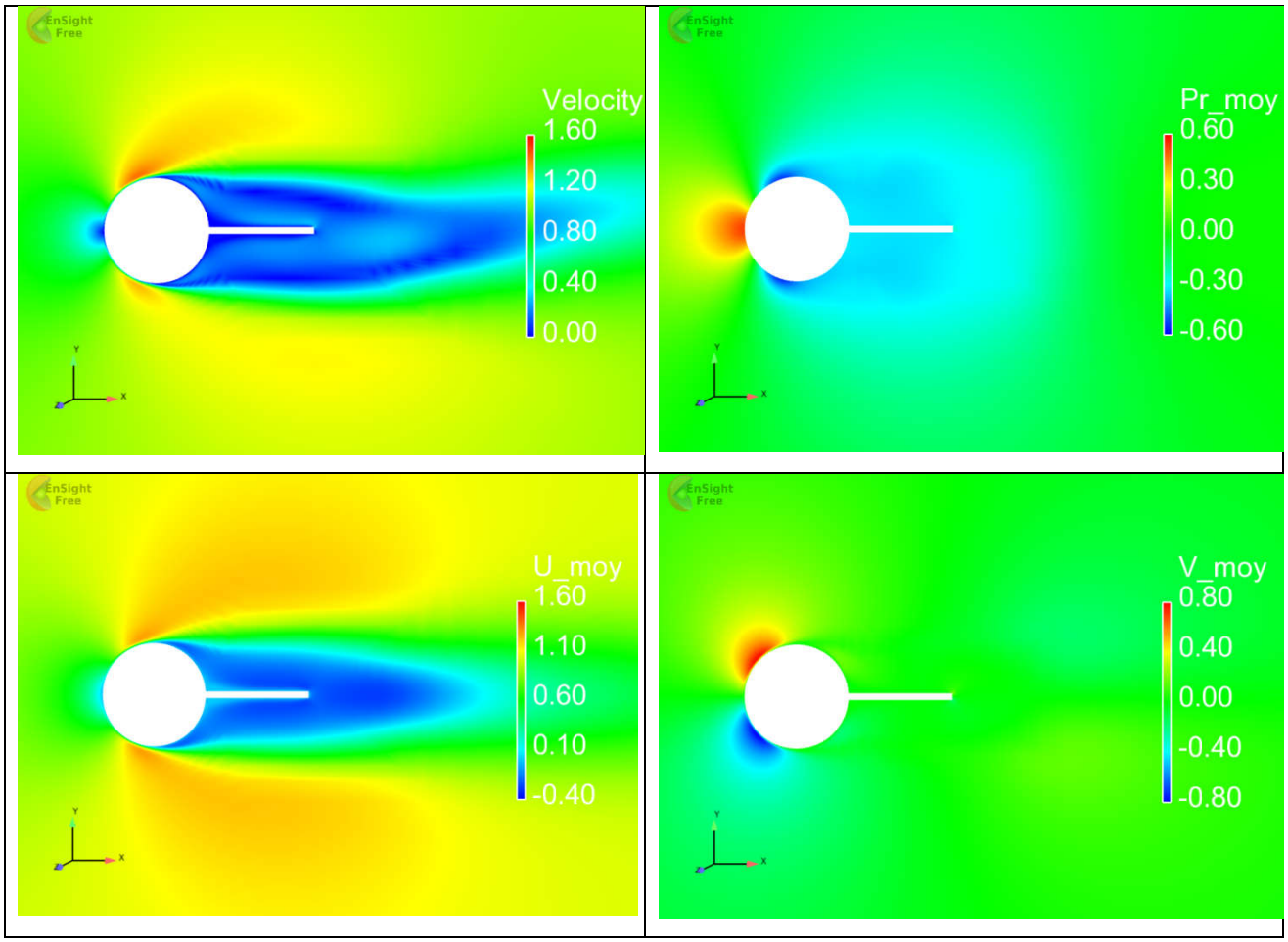

Fig. 5.21 Different fields of the flow

The figure 5.21 Shows the quantities of flow (mean velocity and pressure fields) of the present study results where: we noticed that we have same pressure distribution and Mean cross-stream velocity (V_moy) with the other cases smooth cylinder (figure 5.7) and grooved cylinder (figure 5.14). While in local velocity and Mean stream-wise velocity (U_moy), the recirculation zone is longer than other cases.

GENERAL CONCLUSION

General conclusion

In this work, we used the numerical simulation provided by the free software Code_Saturne to study the behavior of flow around a single cylinder, with geometrical shape modification. The objective of this work is to investigate the effect of cylinder's geometrical shape modification on properties of flow which are velocity, pressure distribution and aerodynamics forces (drag/lift). For this study, we performed simulations in three different forms, which are smooth cylinder, grooved cylinder and cylinder with flat plate. We used $k-\omega\ SST$ as turbulence model. The geometry and the boundary conditions are the same for all tested cylinders. And in order to be able to compare our results with experimental studies, therefore we chose a different Reynolds number for each case.And we made a mesh sensitivity test with a comparison of four grids (coarse, medium, fine and very fine) was carried out, to define the best grid to use for our simulation.

The first case concerns a simulation of a flow around a smooth cylinder. We have shown a comparison of our simulation with the experimental results. After presenting the simulation results we plotted the average velocity in the wake axis and we presented the mean stream-wise ($U/U0$) and crosse-stream ($V\ /\ U0$)velocity profiles respectively, in the wake cylinder at three points, and then we plotted the distribution of Pressure Coefficient around the surface of a cylinder. We followed the same steps in the grooved cylinder case. As for the third case (cylinder with plate) we could not perform a comparison because the absence of experimental data, so we only presented our numerical results.

Finally, the results obtained in the first and second cases are in good agreement with the experimental and numerical results. In addition, there is some notice need to mention. When we plotted the average velocity curve we observed that the cylinder with plate has the highest minimum velocity, the loop length and the maximum return speed are less than other cases. While in the grooved cylinder we have a small loope length, and high return speed than other cases. And that return to the effect of the grooves and splitter plate.

It was supposed to be a fourth case which is wavy cylinder, and investigate the drag reduction, but unfortunately there was not enough timeto perform all those parameters.

BIBLIOGRAPHY

[1]Zhang H. L. andKo N.W.M. (1996). Numerical analysis of incompressible flow over smooth and grooved circular cylinders.Comput. Fluids 25, 263–281

[2]Kim J. and Choi H.(2005).Distributed forcing of flow over a circular cylinder.Physics of Fluids 17, 033103.

[3]Rahman M. M., Karim M. M. and Alim M. A.(2007).Numerical investigation of unsteady flow past a circular cylinder using 2-d finite volume method.Journal of Naval Architecture and Marine Engineering, 4(1), 27–42.

[4]Razavi S. E., FarhangmehrV. and BararF. (2008). Impact of splitter on flow and heat transfer around circular cylinder at low reynolds numbers.Journal of Applied Sciences, 8: 1286-1292.

[5]Lam K. and Lin Y. F.(2008).Large eddy simulation of flow around wavy cylinders at a subcritical Reynolds number. Intl J. Heat Fluid Flow 29, 1071–1088.

[6]Afgan I., Kahil Y., BenhamadoucheS. and Sagaut P.(2011).Large eddy simulation of the flow around single and two side-by-side cylinders at subcritical Reynolds numbers.Physics of Fluids 23, 07510.

[7]Ladjedel A.O., Yahiaoui B.T., Adjlout C.L. and Imine D.O. (2011).Experimental and Numerical Studies of Drag Reduction on a Circular Cylinder. International Journal of Mechanical, Aerospace, Industrial, Mechatronic and Manufacturing Engineering, 5, 905-909.

[8]Badami P., Shrivastava V., Saravanan V., Hiremath N. andSeetharamuK. N.(2012). Numerical analysis of flow past circularcylinder with triangular and rectangular wakesplitter.International Journal of Mechanical and Mechatronics Engineering, 6(9), 174.

[9]Ladjedel O., Adjlout L., YahiaouiT. and Imine O. (2012). Experimental study of pressure drop reduction on in-line tube bundle using passive control.EPJ Web of Conferences, 25, 01044.

[10]ZOU L., GUO C. and XIONG C.(2013).Flow characteristics of the two tandem wavy cylinders and drag reduction phenomenon. Journal of Hydrodynamics, Ser. B, 25(5), 737-746.

[11]Ladjedel O., Adjlout L., Hachim M. R. ,Razi A. and Yahiaoui T. (2014). Experimental study of flow around two grooved cylinders arranged in tandem.EPJ Web of Conferences, 67, 02066.

[**12]Munendra C. V., Inamdar A., Kumar R.**(2015). Numerical studies of drag reduction on circular cylinder with V-grooves.International Journal of Engineering Research and General Science, 3(3), Part-2.

[13]Liu K. , Deng J. and Mei M.(2016). Experimental study on the confined flow over a circular cylinder with asplitter plate.Flow Measurement and Instrumentation,51, 95-104.

[**14]HE J., ZHAO W. and WAN D.**(2018). Numerical Calculations for Smooth Circular Cylinder Flow at 3900 Reynolds Numbers with SST-IDDES Turbulence Model.ICCM2018, 6th-10th August 2018, Rome, Italy.

[15]Kaur M. and Kumar P.(2018). Numerical investigation of flow over a circular cylinder at different gap ratios.IOP Conference Series Materials Science and Engineering, 402(1), 012156

[16]*Rahmani Z., Kahil Y. etBenlefki A.(*2019). Étude numérique d'écoulement turbulent autour de quatre cylindres en configuration carré. Recueil de mécanique/ASJP, 4 (2), 359-373.

[17]Sun X.,Suh C. S.,Ye Z-H. And Yu B.(2020). Dynamics of circular cylinder with an attached splitter plate in laminar flow: A transition from vortex-induced vibration to galloping. Physics of Fluids 32, 027104.

[18]Menter F. R.(2011).Turbulence Modeling for Engineering Flows.ANSYS Inc. (Technical Paper 25).

[19]Gustavsson H. (2006). Introduction to Turbulence.Division of FluidMechanics, Luleå University of Technology, (Report).

[20] https://www.boldmethod.com/learn-to-fly/aerodynamics/how-to-avoid-wake-turbulence/**:05/09/2021**

[21]http://www.ase.uc.edu/~pdisimil/classnotes/Turbulence2019/ABR_2018TURB_C1B_Charateristics_16Jan2019.pdf **:05/09/2021**

[22] VersteegH. K.and Malalasekera W.(2007). An Introduction to Computational Fluid Dynamics: The finite volume method. 2nd Ed. Pearson Education Limited, England

[23] http://insightreplay.com/tech-sports-computational-fluid-dynamics/**:05/09/2021**

[24] FustéR. P. (2018). Thermal-hydraulic analysis of the ITERElectron Cyclotron Upper Launcher Antenna.Master thesis.EscolaTècnica Superior d'Enginyeria Industrial de Barcelona.

[25]Zuo W. Introduction of Computational Fluid Dynamics. FAU Erlangen-Nürnberg JASS 05, St. Petersburg.

[26] https://www.idealsimulations.com/resources/turbulence-models-in-cfd/**: 05/09/2021**

[27] Nicoud F.(2007). Unsteady flows modeling and computation. University Montpellier II and I3M-CNRS UMR 5149, France, (Report).

[28] Friess C. (2010).Modélisation hybride RANS / LES temporelle desécoulements turbulents. Thèse, Université de Poitiers.

[29]Perron C., Boudreau M., Gauthier É., Gauvin-TremblayO. andCôté P. (2013).La turbulence en CFD : Modélisation et Simulation. Laboratoire de Mécanique des Fluides Numérique, Université de Laval.

[30] SenguptaK.,Mashayek F.and Jacobs G. (2008). Direct Numerical Simulation of Turbulent Flows Using Spectral Method. 46th AIAA Aerospace Sciences Meeting and Exhibit.07-10 January 2008, Reno, Nevada.

[31]Shinjo J.andUmemura A. (2010). Simulation of liquid jet primary breakup: Dynamics of ligament and droplet formation. International Journal of Multiphase Flow, 36 (7), 513-532.

[32] Wilcox D. C. (2006).Turbulence Modeling for CFD, 3rd edition, DCW Industries,Inc, California, USA.

[33] https://www.cfd-online.com/Wiki/SST_k-omega_model

[34]Geuzaine C. and RemacleJ. F.(2009). Gmsh: a three-dimensional finite element mesh generator with built-in pre- and post-processing facilities. International Journal for Numerical Methods in Engineering 79(11), 1309-133. (https://gmsh.info/)

[35] https://www.code-saturne.org/cms/

[36] https://www.qantur.com/computational-fluid-dynamics/ansys-ensight

[37]https://www.directindustry.fr/prod/ansys/product

[38] https://www.paraview.org

[39]https://docs.paraview.org/en/latest/UsersGuide

[40]https://plasma-gate.weizmann.ac.il/Grace/doc/UsersGuide

[41]Yahiaoui T., Ladjedel O., Imine O. andAdjlout L. (2015). Experimental and CFD investigations of turbulent cross-flow in staggered tube bundle equipped with grooved cylinders.Journal of the Brazilian Society of Mechanical Sciences and Engineering, 38(1), 163–175.

[42]NorbergC. (2002). Pressure Distributions around a Circular Cylinder in Cross-Flow. Conference: Symposium on Bluff Body Wakes and Vortex-Induced Vibrations (BBVIV3)At: Port Arthur, Queensland, Australia.

[43] Parnaudeau P., Carlier J., Heitz D. and Lamballais E. (2008).Experimental and numerical studies of the flow over a circular cylinder at Reynoldsnumber 3900. Physics of Fluids 20, 085101.

Abstract:

This work aims to study the behavior of flow over cylinders with geometrical shape modification. We study the flow by the RANS approach using the Code_Saturne to solve the system of equations governing the flow. We performed simulations for three cases, which are smooth cylinder with Reynolds number 3900, grooved cylinder with Re = 9300 and cylinder with flat plate in Re = 3000. We used the turbulence modelnamed $k-\omega\ SST$. After comparing the results obtained from our study with the previous results, we concluded that each cylinder shape has a special effect on the flow behavior. We can benefit from each cylinder in different applications.

Key words:

Turbulent flow, smooth cylinder, grooved cylinder, RANS, Reynolds number, cylinder with plate.

ملخص:

يهدف هذا العمل إلى دراسة سلوك التدفق فوق الأسطوانات مع تعديل الشكل الهندسي. ندرس التدفق من خلال نهج RANS باستخدام Code_Saturne, لحل نظام المعادلات التي تحكم التدفق. أجرينا عمليات محاكاة في ثلاث حالات. وهي أسطوانة ملساء برقم رينولدز3900 ,وأسطوانة محززة ب9300 وأسطوانة ذات صفيحة ب3000. استخدمنا نموذجالاضطرابSST ω – k.بعد مقارنة النتائج التي تم الحصول عليها من دراستنا مع النتائج السابقة, خلصنا أن لكل أسطوانة لها تأثيرها الخاص في التدفق. يمكننا الاستفادة من كل أسطوانة في تطبيقات مختلفة.

الكلمات المفتاحية:

التدفق المضطرب ، الأسطوانة الملساء ، الأسطوانة المحززة, RANS ، رقم رينولدز ، الأسطوانةذات صفيحة

Résumé

Ce travail vise à étudier le comportement de l'écoulement sur des cylindres avec modification de la forme géométrique. Nous avons étudié l'écoulement par l'approche RANS en utilisant le Code_Saturne pour résoudre le système d'équations régissant l'écoulement. Nous avons effectué des simulations pour trois cas, qui sont : un cylindre lisse avec le nombre de Reynolds 3900, un cylindre rainuré avec Re = 9300 et un cylindre avec plaqueà Re = 3000. Nous avons utilisé le modèle de turbulencek − ω SST. Après avoir comparé les résultats obtenus de notre étudeavec les résultats précédents, nous avons conclu que chaque cylindre a un effet particulier sur le comportement de l'écoulement. Nous pouvons profiter de chaque cylindre dans différentes applications.

Mots clés:

Écoulement turbulent, cylindre lisse, cylindre rainuré, RANS, nombre de Reynolds, cylindre avec plaque.

remarks	
In chapter 2, we presented very large information that was not used in core of the work. And we present the equation in 3D form while the simulation performed in 2D form.	In Chapter 2, we conducted a general study on turbulence modeling. We provided a lot of information and mentioned different turbulence models to make our manuscript useful to other students next years.
The calculation convergence in the case of the smooth cylinder require a little more analysis as well as the number of iteration	The calculations performed in 10000 iteration with time step 0.1(for that the figures displayed $time(s) = 1000$). I think it was enough to get good results.
The comparison of pressure coefficient with a different Reynolds number (3000and 3900).	3000 and 3900 are in same Reynolds numbers range, so our comparison is existed. And there are many articles performed same comparison.